BIRD STREAMER INITIATED BREAKDOWN UNDER HVDC CONDITIONS

by

Kribashen Naidoo

(B.Sc. Electrical Engineering)

A dissertation submitted in partial fulfilment (50 %) for the requirements of the degree of

Master of Science in Electrical Engineering

In the

School of Electrical, Electronic and Computer Engineering

Faculty of Engineering

University of KwaZulu-Natal.

South Africa

29 January 2007

Supervisors:

Professor N.M. Ijumba

Professor A.C. Britten

DECLARATION

I, the undersigned, hereby declare that the material presented in this dissertation, entitled ***"Bird Streamer Initiated Breakdown under HVDC Conditions",*** is my own work, except where specific acknowledgement is made in the form of a complete reference.

.....

K. Naidoo

.....

Date

As the candidate's supervisor, I have/have not approved this dissertation for submission.

Signed: .....

Name: .....

Date: .....

To my family,

especially my parents!

ACKNOWLEDGEMENTS

The work presented in this dissertation was carried out under the supervision of Professor N.M. Ijumba of the University of KwaZulu-Natal, and Professor A.C. Britten of ESKOM. I wish to thank Professors Ijumba and Britten for their encouragement and guidance provided to me throughout my studies.

A special thank you is also due to:

(i) My fiancée Tanya Naidu, for her great love, understanding and patience during the past year.

(ii) The staff of the HVDC Centre, for their support during my studies.

(iii) THRIP and ESKOM, for providing financial support.

I would lastly like to thank *GOD,* for allowing me to complete this dissertation.

ABSTRACT

This dissertation describes the role played by bird streamers in transmission line faults under HVDC conditions. The research was initiated due to the lack of knowledge of these faults under HVDC conditions. An explanation as to what bird streamers faults are, the role they play in the breakdown of air-gaps and a means of preventing bird streamer caused faults from occurring is made

Experimental work has been carried out in order to gain an understanding of these faults under HVDC conditions. The overall aim of the experiments was to find a horizontal distance (protected zone) on an HVDC tower top, in order to prevent birds from perching around the centre of the tower. This will lead to a reduction of bird streamer caused faults.

A brass rod was used as the artificial streamer in the experiments, under both negative and positive polarity (voltages in the range 0 to 220 kV DC were applied). Later in the experimental phase, a string soaked in a saline solution was used as a more realistic simulation of a bird streamer.

QuickField^{TM}, an FEM package, was used to simulate the electric field in the region of the live conductor fitting and the tip of the bird streamer, to assess the degree of distortion of the electric field caused by the introduction of the bird streamer. These simulations served as means of verifying the laboratory experiments.

This dissertation has proposed a relationship between the breakdown voltage and the protected zone length, based on the air-gap breakdown voltages for both I-String and V-String insulator configurations in the air-gap range 0 to 350 mm. These curves can be used in the design of transmission lines, as a means of reducing bird streamer faults.

CONTENTS

LIST OF FIGURES

LIST OF TABLES

LIST OF ABBREVIATIONS

General

HVAC	High Voltage Alternating Current
HVDC	High Voltage Direct Current

Organizations

BPA	Bonneville Power Association
EPRI	Electric Power Research Institute (United States)
ERIC	Eskom Research and Innovation Centre
FPL	Florida Power and Light
IEE	Institution on Electrical Engineers
IEEE	Institution of Electrical and Electronic Engineers
UKZN	University of KwaZulu-Natal

LIST OF SYMBOLS

α	ionisation coefficient
$\acute{\alpha}$	effective ionization coefficient
η	attachment coefficient
δ	relative air density
^0K	degree Kelvin
^0C	degree Celsius
b_0	air density
d	gap length
D	primary air-gap length
D_1	first air gap length for floating bird streamer
D_2	second air-gap length for floating bird streamer
E	electric field
E_{arc}	electric field of the arc channel
E_{av}	average flashover gradient
E_p	electric field of the pollution layer
k_d	air density correction factor
k_n	humidity correction factor
k_t	atmospheric correction factor
L	bird streamer length
n_0	number of electrons emitted by the cathode
n_s	number of electrons at a distance d from the cathode
R_{arc}	resistance of arc channel
R_p	resistance of pollution layer
S	Siemens

S_0	surface between electrodes
t_0	air temperature
T	total length
U_{corr}	breakdown voltage under standard conditions
U_{bkd}	breakdown voltage under test conditions
V_{HVDC}	applied HVDC
x	distance in the x direction
x_c	critical avalanche length

1 INTRODUCTION

1.1 Background knowledge

It has been widely documented that the first power generation station (by Thomas A. Edison) was direct current (DC), which began operation in the United States of America in 1882. In the same year, the first high voltage direct current (HVDC) transmission system was built, which transmitted 1.5 kW at a voltage of 2 kV over a distance of 58 km [1]. However, during this period, voltage conversion proved to be a difficult task, due to the lack of available technology.

In an AC system, voltage conversion is a simple process, performed by means of a power transformer. The advent of the induction motor and polyphase circuits further developed AC systems.

For a long time, AC systems remained the only means for power transmission and distribution because of their inherent advantage of changing one voltage level to another. However, they do have certain drawbacks associated with them. For example, a connection between two different frequencies is impossible to achieve, and secondly, the inductive and capacitive elements of overhead lines and underground cables limits the transmission capacity [2].

In the past few decades, a significant amount of research has been carried out to develop DC transmission and distribution systems technology in order to supplement AC systems. A key factor that accelerated this research work was the advent of semiconductor devices, notably the thyristor.

This led to the installation of the first commercial HVDC system in Sweden, in 1954, which resulted in many more HVDC systems being set up around the world [3].

A number of faults occur on HVAC systems, many of which have been well researched, and, therefore, understood. Faults in HVDC systems, on the other hand, have been far less researched, due to the small number of these systems around the world as compared to AC systems [3].

This research project is based on a specific problem that occurs in HVAC networks, but has not yet been identified as a major problem in the HVDC case. The problem relating to faults caused by birds has been documented for many years, under the *unidentified* category of fault types in the HVAC case [4]. In this dissertation, focus will be on a bird streamer as a possible initiator of flashover under HVDC stress. In other cases birds can cause faults through the pre-deposition of excreta on insulators, leading to flashover across the insulator string [4].

Bird streamer caused faults and pre-deposition faults accounted for about 34% and 4% respectively, of all faults on the 275 kV AC transmission grid in the Republic of South Africa (RSA) between the periods 1996 to 1999 [4].

Considering the current situation in RSA; there exists a single HVDC link (± 533 kV) between RSA (Apollo Converter Station) and Mozambique (Songo Power Station), with the possibility of future major transmission links between RSA and the Democratic Republic of Congo (DRC). There is also a possibility of the uprating of the Apollo-Songo to a voltage of 600 kV.

Bird streamer faults have not yet been identified as a major cause of faults in the South African side of the above mentioned HVDC link, nor are they believed to be so in Mozambique [5]. Figure 1.1 shows the distribution of fault types on the South African side of this line for the period 01/01/2001 to 30/09/2005.

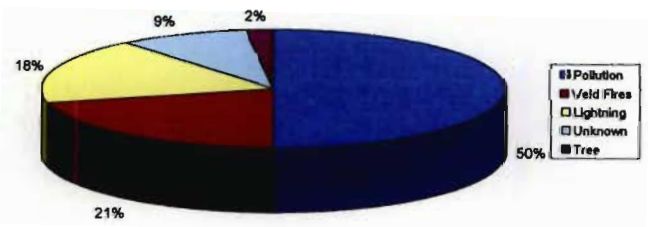

Figure 1.1 Causes of line faults on the South African side of the Apollo-Songo HVDC link, *(reproduced from [5])*

Figure 1.1 shows that the causes of 9% of all faults are unknown (i.e. the cause of the fault are unidentified); therefore there exists a possibility whereby, a bird streamer may fall into this unknown region (detailed in Chapter Two).

Thus in order to provide support for existing and future HVDC systems, much emphasis has top be placed on research into HVDC systems design and operation.

1.2 Research problem definition

The following section provides an understanding of the possible problems associated birds and HVDC lines, and more importantly directs attention towards the research problem, and the objectives of this study.

1.2.1 Research problem

In the HVAC case, a bird streamer fault is caused by a conducting stream of liquid excreted by a bird perching on a tower top. This stream is at a ground potential due to the contact between the bird and the grounded tower top. As it approaches the live conductor fitting, it may lead to flashover between the grounded tower top and the nearest live hardware.

The bird streamer fault has two key identifiers:

(i) A flashmark caused by a power arc generated by the bird streamer, and

(ii) The time of occurrence of the fault.

The flashmark is in most cases situated on the steel crossarm of the tower, in the region above the live conductor, and at the live end of the insulator string, as shown in Figures 1.2(a) and 1.2(b) respectively.

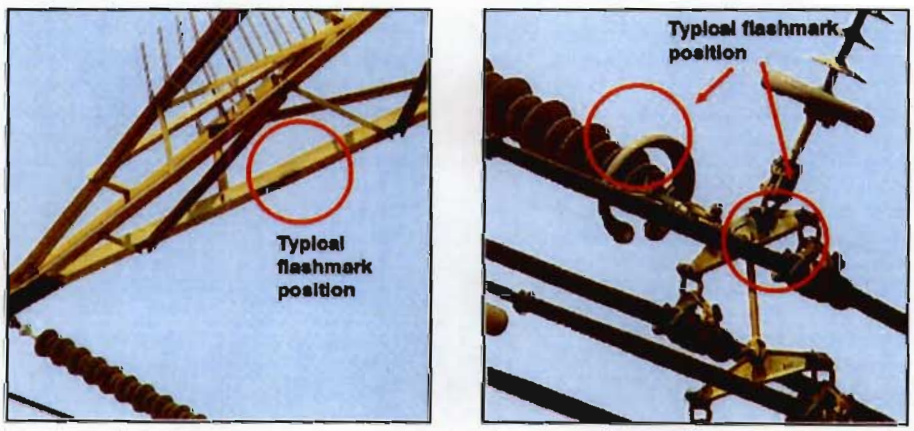

(a) On the steel tower (b) On the live hardware

Figure 1.2 Typical flashmark observations, *(selected from [4])*

The occurrence of bird streamer type faults tend to follow a *bimodal distribution*, with peaks in early evenings (between 18h00 and 23h00) and again in early mornings (between 04h00 and 08h00). Birds generally forage during the periods between 08h00 and 18h00, thereafter

returning to the tower tops, which provide a safe perching environment. On leaving the tower tops in the early parts of the morning (between 04h00 and 08h00), they generally defecate, and in certain cases, this may lead to a bird streamer caused fault [4]. This could provide an understanding as to why these bird related faults occur in these periods.

Based on a comprehensive literature survey (undertaken in Chapter Two), a conclusion has been reached which postulates that under an *essential* condition, the introduction of a bird streamer into the V-String or I-String insulator configurations on an HVDC tower top may cause a breakdown of the air-gap between the bird streamer tip and the live conductor fitting, thereby leading to a line to ground fault. Further discussion of this *essential* condition will be covered in Chapter Two.

As a means of preventing bird streamer caused faults on 275 kV and 400 kV AC lines, Taylor [6] developed the concept of a forbidden or protected zone on a tower top (shown in Figure 1.3). Figure 1.3 shows this concept for a V-String insulator configuration; this can also be applied to an I-String insulator configuration. This zone is a region on the tower that should be protected from birds. By doing this, the bird streamer caused fault is reduced. This has not been applied to the HVDC scenario.

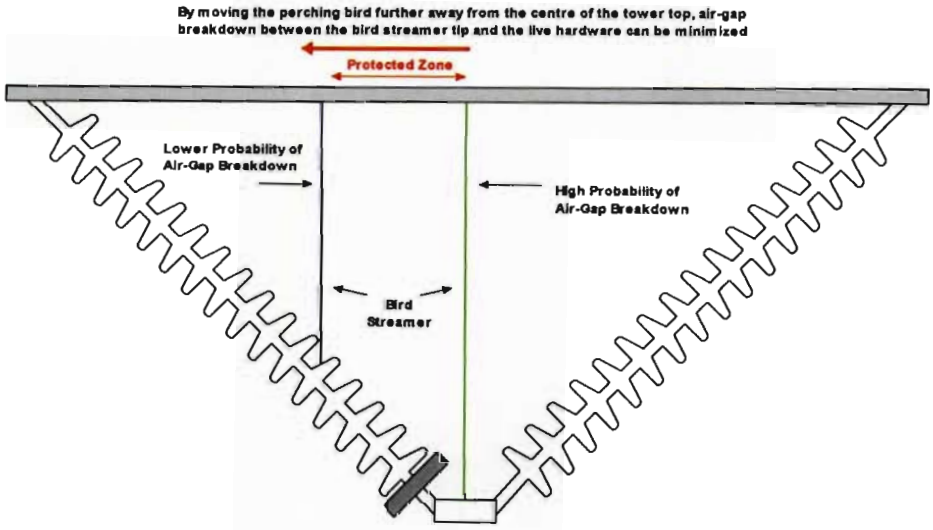

Figure 1.3 Bird streamer fault minimisation process

1.2.2 Objectives of the research

This research, has therefore investigated the characteristics of a bird streamer being introduced into a V-String and I-String insulator configuration and its effect on the HVDC tower insulation strength. *Specifically*, the study has:

(i) Investigated the effects of the reduced insulation strength caused by a bird streamer being introduced into a V-String and I-String insulator configuration on an HVDC and HVAC tower.

(ii) Quantified the factors that lead to breakdown namely the conductivity of the excreta and the length of air-gap between the tip of the bird streamer and the live conductor fitting.

(iii) Considered both positive and negative polarities (each in a mono-polar configuration).

(iv) Developed a curve that displays the relationship between breakdown voltage and protected zone length for HVDC and HVAC towers. This protected zone length is a horizontal length on a tower top; the length of which was formulated from experimental work. This is the zone where bird deterrents are to be placed, in order to prevent bird streamer faults from occurring.

1.3 Motivation for the research

In recent times, utilities around the world and more importantly Eskom have shown an eager interest in investigating the mechanisms and parameters of bird streamer faults, which have been classified as unidentified faults. On the other hand, such faults in the DC case have not been given the same attention.

The disruptive nature of HVDC faults, and more importantly, its highly repetitive nature, could cause a loss of a converter, thus leading to the loss of power. This type of fault is much more severe than HVAC faults. It is therefore essential to understand the bird streamer related

phenomenon at an early stage for the improved design, and hence minimisation of faults and therefore provide reliability of current and future HVDC transmission and distribution systems.

1.4 Research methodology

1.4.1 Literature review

The literature survey was based on past knowledge gained on bird streamer faults and the breakdown characteristics of air-gaps under DC and AC conditions. New ideas and questions relating to the research problem were founded from the survey; aiding substantially in the understanding of the research problem, which led to the development of a solution method.

1.4.2 Laboratory experiments

A series of laboratory experiments were undertaken in order to elucidate the problem. The equipment needed in the experiments included the construction of a model HVDC tower. Also constructed was an apparatus used for the injection of an *artificial* bird streamer (brass rod and saline soaked string). This system allowed for controlled lengths of the streamers to be generated (using a static insertion method).

The model tower was used to determine the air-gap insulation strength, and thus the role of streamer conductivity on air insulation strength. These experiments were aimed at aiding in the calculation of the protected zone length.

1.4.3 Electric field analysis

In order to verify the experimental results, further work was done utilising the finite element method (FEM), in the form of a field simulation software named QuickField™. This model looked at the electric field intensity between the streamer tip and the live conductor fitting, as the streamer descends towards the live conductor fitting.

1.5 Structure of the dissertation

The following points summarise the content of the respective chapters in this dissertation:

(i) *Chapter Two* outlines the literature applicable to the research problem posed in section 1.2. This chapter details past work relating to bird caused outages. A survey of air-gap breakdown phenomena is also presented. An overall view of the bird streamer phenomenon modelled as an air-gap breakdown process is explained.

(ii) *Chapter Three* explains the research methodology followed in the research project. The experimental apparatus and procedures followed in the research are explained in detail. A discussion of the electric field simulation software and the associated geometric model is made.

(iii) *Chapter Four* details the experimental results into air-gap breakdown under DC conditions. A comparison of the DC results is made with results obtained under AC conditions. This chapter also looks as the electric field simulation results. A thorough discussion and application of the results is also undertaken.

(iv) *Chapter Five* provides a summary of the results obtained and the conclusions reached from the project. Possible further work to be executed in this research area is also mentioned.

2 LITERATURE REVIEW

2.1 Introduction

The focus area of the assessed literature was based on the following topics:

(i) Local and international utilities experiences and research initiatives in dealing with bird related faults under HVAC and HVDC conditions.

(ii) Electrical discharge phenomena and air-gap breakdown characteristics.

2.2 Bird related faults

This section provides an analysis of past work regarding bird related faults under HVAC conditions. Details of the laboratory and field work are indicated, together with the outcomes of the respective work. Mention is also made of the unidentified faults experienced along the Apollo-Songo line.

The earliest form of research work relating to bird faults goes back to the early 1920s, performed by Michener [7]. The work comprised laboratory experiments using bird excretement to initiate a flashover. Field studies were utilised, whereby protective devices were installed to prevent excretement from contaminating insulators.

This was the first of recognition given to faults caused by bird streamers. The following paragraphs detail relevant information, leading to current practices and research initiatives related to bird steamer faults.

Bonneville Power Association (BPA) [8] initiated full scale experimental tests in 1971, in order to get an understanding of the flashover mechanism associated with bird excretement. BPA in association with the United States Electrical Power and Research Institute (EPRI) [9] also investigated the anomalous transmission line outages in the late 1980s. This research work concluded that bird streamer faults were *not* a major contributing factor to the total number of line faults, but on the other hand they could *not* be discarded as a possible cause of line faults.

Burnham [10] investigated the bird streamer flashover mechanism as a possible cause of the excessive outages experienced on Florida Power and Light (FPL) transmission lines. The AC

networks considered in the investigation were 138 kV, 270 kV and 500 kV. The research concentrated on the *time of day* analysis of the faults. Burnham categorized the number of fault types with the hour of day that the fault occurred. This analysis proved to be a vital tool in determining the cause of the line faults.

In his findings, Burnham showed that the faults caused by bird streamers and the faults caused by pollution occurred at a similar time of the day (i.e. between 22h00 and 06h00). This, according to Burnham, was the determining reason for ignoring bird related faults in previous times.

The work performed by Burnham marked the beginning of in depth studies into bird streamer faults.

Taylor [6] undertook an investigation to determine the root cause of the increased number of faults on the 275 kV AC transmission grid in South Africa. In his study, Taylor identified the burn or flash marks caused by power arcs on tower tops; this was considered to be an indication of bird streamer caused flashovers and not pollution related faults. The work entailed experimental testing of simulated solid bird streamers from tower tops, and by doing this, provided a minimum flashover distance for AC system voltages. The artificial streamer consisted of a brass rod with diameter 12 mm, and string soaked in a saline solution, with conductivities of 25 $mS.cm^{-1}$ and 10 000 $\mu S.cm^{-1}$. The experimental work was used to calculate a protected zone length on a tower top, which was 900 mm from the centre of a V-String insulator configuration (i.e. 1800 mm in total).

As a follow up to the work performed by Taylor, Hoch *et al.* [11], used artificial liquid streamers to investigate faults on the 275 kV and 400 kV AC networks. The artificial streamer was produced using a purpose built apparatus. The apparatus produced liquid streams of diameter 3 mm, with a conductivity of 25 $mS.cm^{-1}$. The research determined a minimum tower top distance in order to prevent flashover at system voltages in the range 88 kV to 275 kV (details of these distances are provided in Table 4.1).

A comparison of the work performed by Taylor and Hoch *et al.* (i.e. the AC case) and the work performed by the present author will be given in Chapter Four.

Investigations into bird streamer flashovers at a system voltage of 400 kV AC was undertaken by Seifert [12]. These investigations looked at the dependence of bird related flashovers on the time of day *and* month. Statistical data obtained from the relevant utilities were used in this research. The unknown faults were investigated on the premise that they were actually bird streamer faults. Most incidents were noted in the early hours of the morning, which was explained as *food biotype behaviour*. This means that during the early hours of the morning, birds leave tower tops in search of food, dropping their excreta just before flying off. This research work explained that the main factor influencing the flashover is due to a decrease in arcing distance.

Wang [13] performed work on insulator flashover mechanisms caused by bird droppings. This work consisted of flashover tests on an I-String insulator configuration at a voltage level of 110 kV AC. The artificial streamer in this case was produced by a purpose built experimental apparatus, the streamer diameter used was 8 mm, and the conductivity of the streamer ranged from 500 $\mu S.cm^{-1}$ to 80 000 $\mu S.cm^{-1}$. Wang found that when the streamer conductivity was greater than 10 000 $\mu S.cm^{-1}$, the probability of flashover was 100 %.

Wang's work highlights the point that the bird streamer causes a distortion of the electric field in the region surrounding the insulator and the live end fitting, in most cases resulting in a flashover. Mention was again made of the lack of evidence of bird droppings on the insulator string following flashover, which provides a reason for ignoring bird related faults in the past.

Recent work relating to bird related outages was performed by Sundarajan *et al.* [7, 14]. The purpose of the work was to review current practices and procedures that were vital in reducing bird related faults. The mitigating techniques put forth were that of perch guards and the regular washing of insulator strings. The perch guards are commonly used by Eskom as a means of preventing bird related faults.

Bologna [5], undertook an investigation into the causes of unknown faults on the South African side of the DC link between South Africa (Apollo Converter Station) and Mozambique (Songo Converter Station). This study utilised both the time-of-day approach as well as field investigations in order to categorise each fault type. This analysis was done so as to look into

the similarities between AC and DC fault types, and thus provide an understanding of the causes of the unknown faults in the DC case, based on historical experience in the AC case.

Figure 2.1 shows the association between the number of faults and the hour of day (a time-of-day curve).

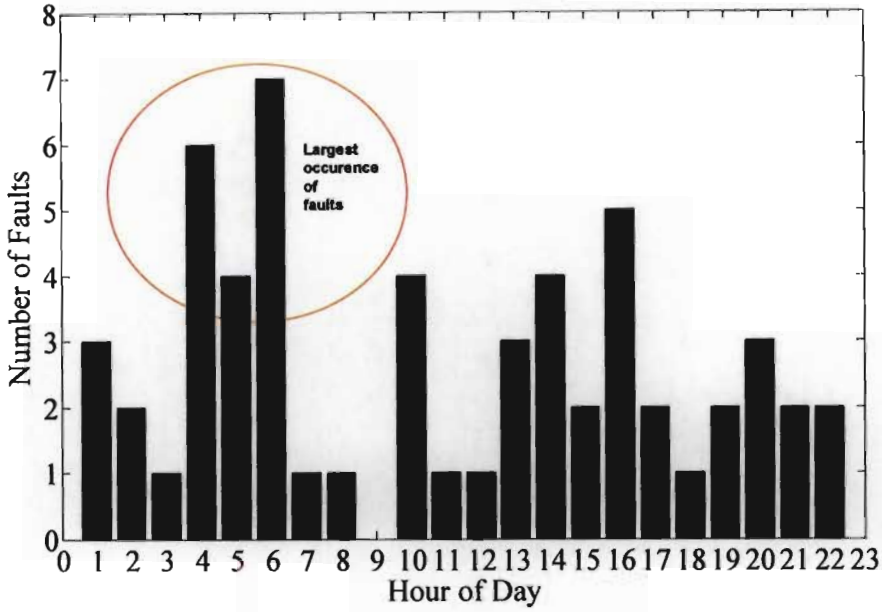

Figure 2.1 Time-of-day occurrence of faults on both positive and negative lines, *(reproduced from [5])*

It can be seen that a majority of the faults occurred at a period from 04h00 to 06h00 in the morning. This trend is similar to that of the time of occurrence of faults mentioned in [4] and [12]. This therefore minimises the faults occurring during this period to either pollution or bird streamer faults. Therefore, one cannot dismiss the possibility of faults occurring at these times being caused by bird streamers.

2.3 The mechanism of the electric discharge

2.3.1 Introduction

Knowledge of the electric discharge process is essential in understanding the mechanism of air-gap breakdown. This section introduces the theory behind electrical discharges; quoted from a selection of the large array of literature available on this topic [15, 16, and 17]. Later on, a summary of the laboratory work that has been accomplished, by various engineers and physicists in this field is presented. Specific mention is made of streamers and the streamer to leader transition process.

2.3.2 Ionisation processes

The air in our atmosphere is the most used insulating material in modern high voltage systems. Insulating strings on HV towers render mere structural support for the high voltage conductors, while the insulation is provided by air. Air tends to breakdown when it loses its dielectric properties, and thus changes from an insulator to a conductor [15].

The process of a gas discharge is assisted by an increase in the electron concentration in the air, which is termed an ionisation process.

2.3.3 Electrical breakdown in very small gaps

Townsend [16] assumed that the initial growth of current between a plane parallel electrode gap was caused by the production of secondary electrons, through the collision of primary electrons generated from the cathode.

Townsend defined an ionisation coefficient (α) as the number of electron ion pairs produced in the gas by a single electron, in moving through a unit distance in the direction of the applied field. This is described by the following equation:

$$n_d = n_0 e^{\alpha d} \qquad (2.1)$$

where,
d = *gap length*
n_0 = *number of electrons emitted by the cathode*
n_d = *number of electrons at a distance d from the cathode*

The Townsend model investigated noble gases, in which electron attachment can be neglected. When the gas used is air, electron attachment has to be considered, thus Equation 2.1 becomes:

$$n_d = n_0 e^{(\alpha-\eta)d} \qquad (2.2)$$

where,
η = *attachment coefficient*
n_0 = *number of electrons emitted by the cathode*
n_d = *number of electrons reaching the anode per* second

The Townsend model suggests that the time taken for air-gap breakdown to occur should be at least equal to the time taken for an electron to cross the air-gap. Experimental work has disproved this, leading to the development of the *streamer (kanal)* model [17].

Equation 2.2 shows that the number of electrons increases exponentially with distance. This exponential growth of electrons with distance is termed an *electron avalanche*.

The number of electrons in this avalanche head grows at a rate given by [16]:

$$n = e^{\bar{\alpha} x} \qquad (2.3)$$

where,

$\bar{\alpha}$ = *effective ionisation coefficient*
x = *distance in the x direction*

With increasing avalanche length, a critical length is reached, whereby the electric field in the avalanche head becomes equal to the background electric field. This is the transition point from an electron avalanche to a streamer discharge.

The space charge electric field plays an important role in the mechanism of *corona* (explained in section 2.3.5) and spark discharges in non-uniform field gaps [17].

The avalanche to streamer transition takes place when the number of charged particles at the avalanche head exceeds a critical value N_c.

Raether and Meek [17] estimated that an avalanche will convert into a streamer when the number of positive ions in the avalanche head reaches a critical value of about 10^8.

Using this value for positive ions, the critical avalanche length for transition to a streamer is given by:

$$e^{\alpha x_c} = 10^8 \qquad (2.4)$$

or

$$\alpha x_c = 18 \qquad (2.5)$$

where,

x_c = *critical avalanche length*

2.3.4 Uniform electric fields

For a uniform air-gap, shown in Figure 2.2, a streamer will be induced only if the critical avalanche length is less than or equal to the air-gap length [16, 17].

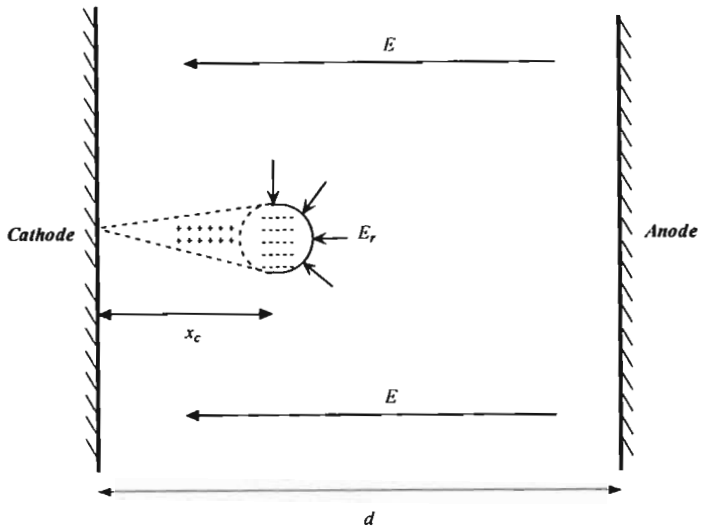

Figure 2.2 Streamer breakdown in a uniform gap, *(reproduced from [16, 17])*

This can be summarised by the following equation:

$$x_c = d \tag{2.6}$$

Using Raether and Meek's criterion for breakdown, this would yield the following equation:

$$\alpha x_c = 18 \tag{2.7}$$

2.3.5 Non-Uniform electric fields

For a streamer to be initiated at the highly stressed electrode and for it to bridge the gap, two conditions have to be met: the first condition is streamer inception, and the second is streamer propagation [16].

An example of a non-uniform field is that of a rod-plane electrode configuration shown in Figure 2.3.

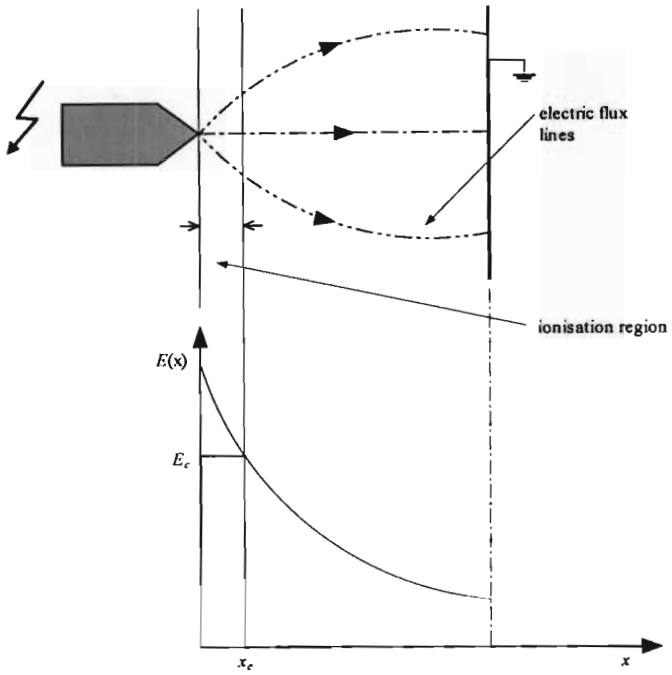

Figure 2.3 Streamer breakdown in a non-uniform gap, *(reproduced from [16, 17])*

The inception criterion of a streamer can be written as:

$$\int_0^{x_c}(\alpha-\eta)dx \geq 18 \qquad (2.8)$$

Secondly, the propagation criterion entails that a specific electric field is required in the air-gap to sustain the streamer propagation.

A great deal of experimental work has been performed in order to calculate the electric field required for streamer propagation. Table 2.1 summarises the streamer propagation criteria found experimentally by Suzuki [18] and Allen *et al.* [19] in the DC case.

Table 2.1 Streamer propagation criteria in the HVDC case

Researcher	*Voltage Stress*	*Air-Gap Length (mm)*	*Electric field required for streamer propagation ($kV.cm^{-1}$)*
Suzuki [18]	Steady HVDC	800 (rod-plane)	5.25
Allen et al. [19]	Steady HVDC	660 (plane parallel)	5.4

From Table 2.1, it is deduced that the electric field required for streamer propagation is $\approx 5\ kV.cm^{-1}$.

2.3.6 Corona discharges

Certain non-uniform electrode configurations result in high electric fields, which results in a discharge phenomenon known as *corona*. A corona discharge occurs long before complete breakdown of the air-gap. During corona discharges, ionic space charge accumulates near the highly stressed electrode thereby modifying the electric field distribution in this region [16].

In small air-gap spacing, direct breakdown is possible without corona inception, but as the air-gap increases in length, the electric field becomes more non-uniform resulting in different corona modes.

The corona discharge is different under negative and positive potentials. Each of the two potentials, produce different corona modes.

The following section provides a summary of the DC corona modes under negative and positive potential adapted from [15, 16].

2.3.6.1 Negative DC Corona Modes

When the highly stressed electrode is at a negative potential, electron avalanches are initiated at the cathode and develop towards the anode in a decreasing field. Free electrons move at a higher rate than the ions in the applied field. This results in a positive space charge around a region of the cathode shown in Figure 2.4.

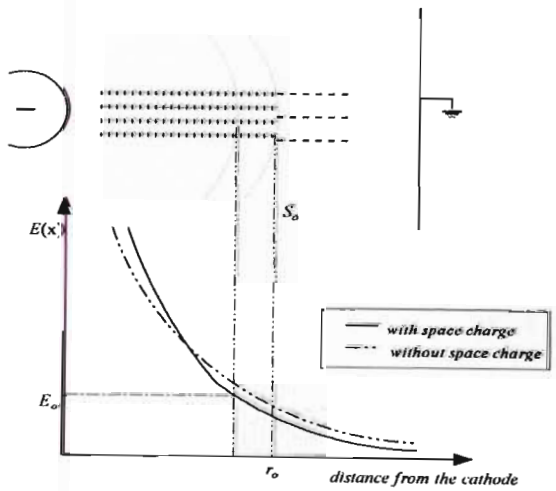

Figure 2.4 Negative corona, *(reproduced from [15, 16])*

The electron avalanche will stop at the surface S_o, where there is a build up of negative space charge. This causes an increase in the electric field in the cathode and a decrease in the anode. This space charge initiation leads to the three different corona modes: Trichel pulses, negative pulses and negative streamers.

Photographs of these different modes are shown in Figure 2.5.

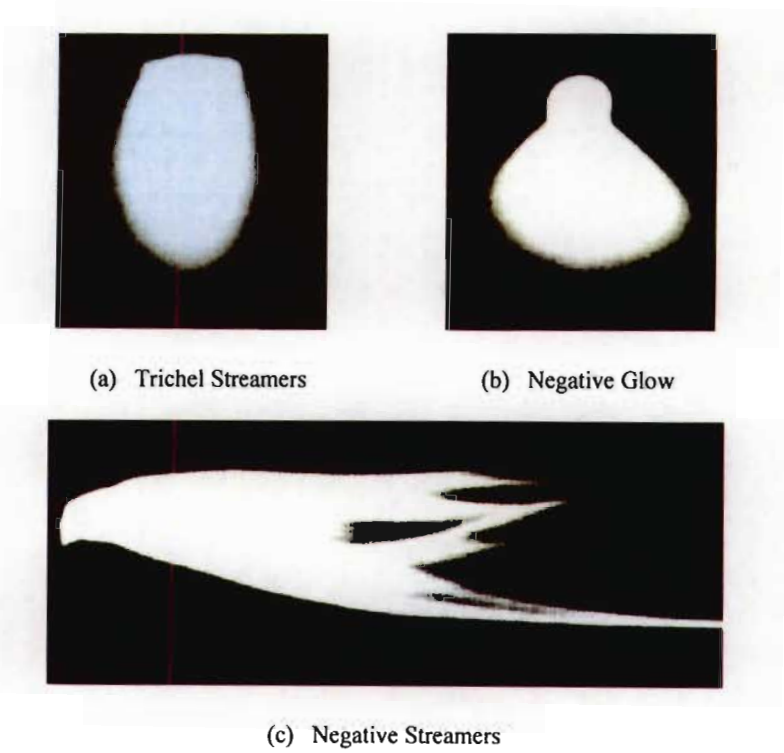

(a) Trichel Streamers (b) Negative Glow

(c) Negative Streamers

Figure 2.5 Negative corona modes, *(selected from [16])*

2.3.6.2 Positive DC Corona Modes

When the highly stressed electrode is at a positive potential, electron avalanches grow towards the anode, shown in Figure 2.6.

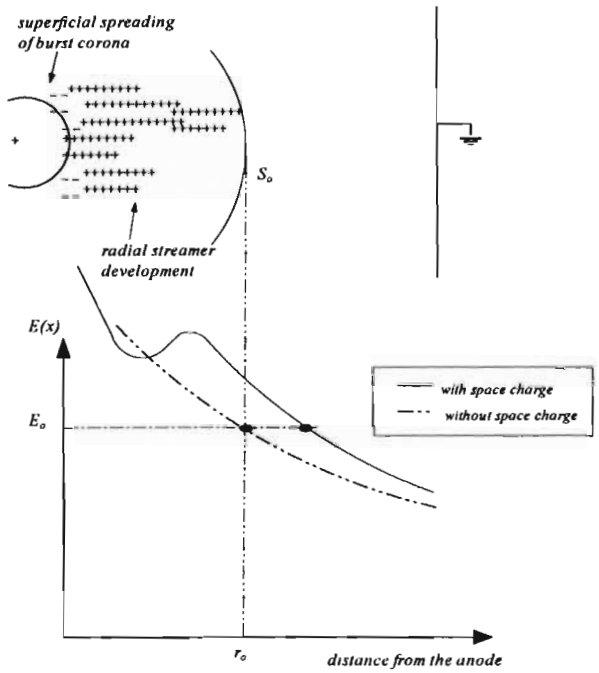

Figure 2.6 Positive corona, *(reproduced from [15, 16])*

The electrons reaching the anode have a high kinetic energy and have to release this energy before they are absorbed into the anode. The loss of energy is in the form of high ionisation activity at the anode. This results in positive space charge being left in front of the anode. A field enhancement is produced in this region, as shown in Figure 2.6.

The positive potential corona discharge has four distinct modes: burst corona, onset streamer, positive glow and breakdown streamers.

Photographs of these different modes are shown in Figure 2.7.

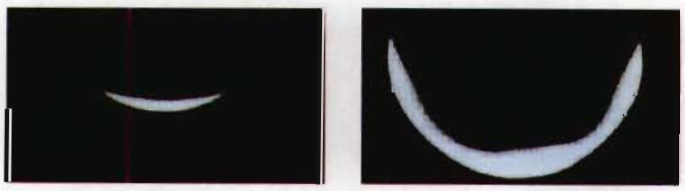

(a) Burst corona (b) Positive (anode) glow

Figure 2.7 Positive corona modes, *(selected from [16])*

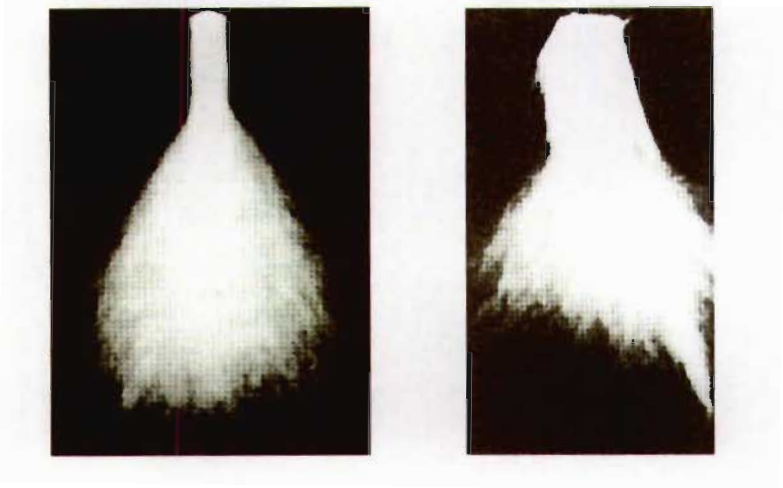

(c) Onset Streamer (d) Breakdown Streamers

Figure 2.7 Positive corona modes, *(selected from [16])*

2.3.7 The effect of polarity on the breakdown process

This dissertation models the air-gap between the bird streamer and the live conductor fitting with the voltage breakdown characteristics of a rod-plane electrode configuration. Due to this relationship, the effect of polarity on the air-gap breakdown of a rod-plane electrode configuration is considered.

A useful explanation of the polarity effect was found in Kuffel *et al.* [17], which is summarised below.

In the case of a positive rod, electrons will be drawn to the anode (rod), thus leaving positive space charge behind the anode region. This space charge causes a reduction in the electric field strength near the anode, while increasing the field further away from the anode. With time, this field extends into the gap extending the ionisation region. The electric field reduction due to space charge can be seen in Figure 2.8.

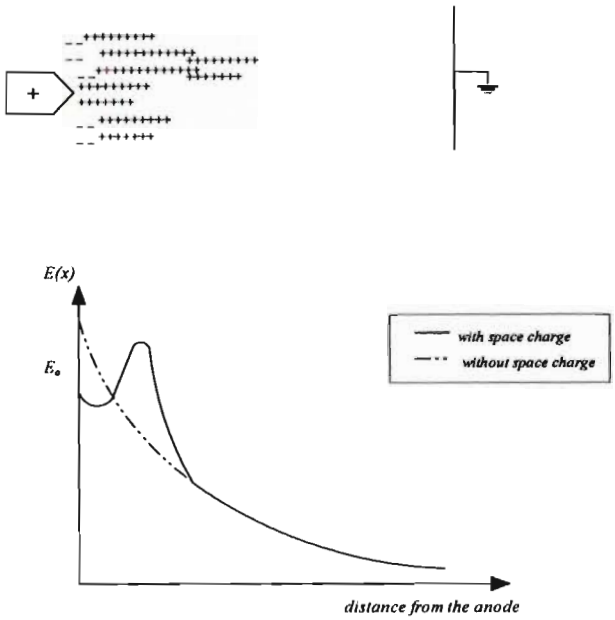

Figure 2.8 Distortion of the electric field, positive rod-plane, *(reproduced from [17])*

In the case of a negative rod, electrons are repelled into the lower field region (anode). In attaching gases (in the present case the gas is air); the electrons are attached to the gas (oxygen) molecules and hold back the space charge which remains in the region between the rod and the negative space charge. The region around the rod has a highly stressed field, but the ionisation in this region is greatly reduced. The electric field distortion can be seen in Figure 2.9. This results in a stoppage of the ionisation process. When this happens, the negative and positive ion space charge is swept away from the region near the rod.

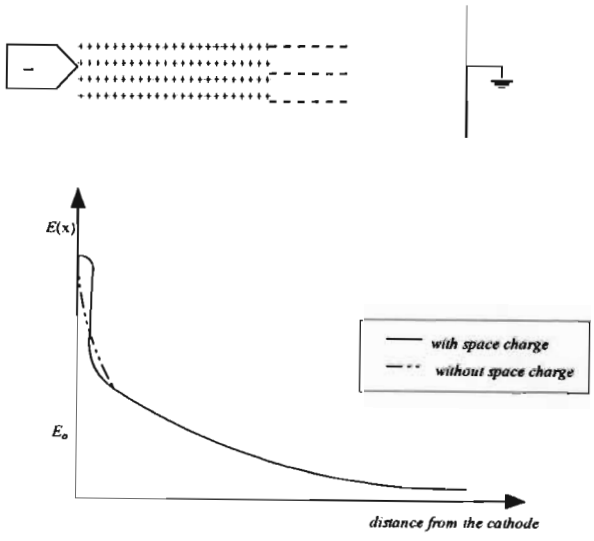

Figure 2.9 Distortion of the electric field, negative rod-plane, *(reproduced from [17])*

A higher voltage is required to overcome this retardation effect. Thus voltage breakdown in the case of a negative point is higher than in the case of a positive point. Applying this result to the case at hand, it would mean that if the plane is energised with positive HVDC, the rod would be at a negative potential with respect to the plane, thus it would require a higher breakdown voltage than when negative HVDC is applied to the plane.

2.3.8 The streamer to leader transition process

For short air-gaps, the streamer to spark transition occurs immediately after the streamer has traversed the air-gap.

In the case of longer air-gaps, a more complicated scenario exists; the following paragraphs provide a summary of this process for a rod-plane electrode configuration, summarised from [16].

The first stage begins with the development of the corona discharge (often called the first corona).

The second stage is the development of a highly conducting channel called the leader channel.

The third stage is where the leader extends, with the aid of corona discharges emanating from the head, towards the grounded electrode.

The final jump starts when the corona streamer emanating from the leader head reaches the grounded electrode.

The streamer and streamer-to-leader transition process has been widely investigated by various other researchers. The research most applicable to this dissertation was selected and the following paragraphs provide a brief account of each of these findings.

Sundarajan *et al.* [20] investigated a dynamic model of the pollution flashover of insulators under DC voltage. This looked at the development of flashover from an arc, and the conditions required for flashover to occur. The polluted insulator model was based on Onenaus' model [20], as shown in Figure 2.10

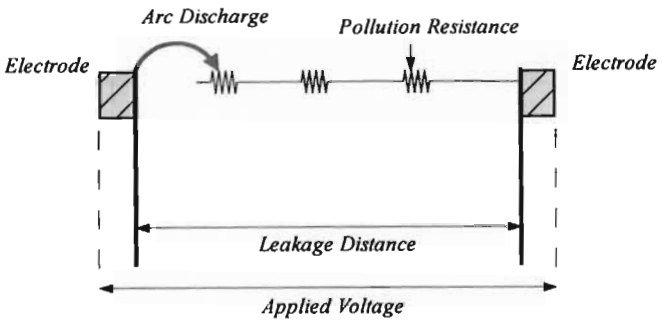

Figure 2.10 Onenaus' model of the polluted layer, *(reproduced from [20])*

The resistance of the pollution layer and the arc are R_p and R_{arc} respectively. In this model, the arc propagation criterion is such that the electric field of the pollution layer (E_p) must be greater than the electric field of the arc (E_{arc}) (i.e. $E_p > E_{arc}$ for arc propagation to occur).

An important point taken from this paper is that the flashover voltage is dependant on the resistance of the pollution layer. A higher pollution resistance results in higher flashover voltage, and vice versa.

Suzuki [21] investigated the transition process from a primary streamer to an arc. The experiments were based on small point-plane air-gaps. The diameter of the points ranged from 0.1 mm to 2 mm, while the air-gap lengths ranged from 1 cm to 4 cm. The experiments detailed the sequence of events from the primary streamer to the thermalization of a highly ionised channel to the arc phase. Suzuki observed that before breakdown occurred, a return ionising wave moves from the cathode to the anode at a speed of 3.6×10^7 cm.sec^{-1}. This results in a relatively small current (1200 to 500 mA) flowing in the air-gap. It was noted that the ionising wave just before the transient process to the final arc, produced electrons densities of 10^{16} cm^{-3}. This occurred within a few nano seconds.

A similar observation was made by Marode [22], but in his work, the velocity of the return wave measured 1×10^9 cm.sec^{-1}.

Larsson [23] investigated the effect of a large series resistance on the streamer-to-park transition. This large resistance is used in HV testing to protect HV sources. The experimental setup consisted of a rod-plane air-gap configuration, energised with HVDC. Three values of a resistor were used: 0, 600 Ω and 6 MΩ. The experiments concluded that the effect of the

inhibiting resistance has *no* influence on the streamer inception voltage, but *does* delay the streamer-to-spark transition process.

Aleksandrov *et al.* [24] studied the effect of a low DC voltage on the development of streamer breakdown in long air-gaps. This theoretical study looked at the possibility of a low DC voltage as a means of completing the streamer to arc transition process (a process initiated by an impulse voltage). It was suggested that if the channel had been heated to a temperature of 300 ^{0}K by the impulse voltage, then the possibility of a low DC voltage culminating the transition process was possible.

Aleksandrov *et al.* [25] also investigated the leader propagation in long air-gaps. A kinetic model was developed to analyse the ionisation process in high temperatures and in strong electric fields. The model looked at the influence of the electric field and gas temperature on the ionisation kinetics. The result of the kinetic model provided evidence in line with previous researchers that the leader bridges very long gaps ($\approx$200 m) at moderately high voltages (< 5 MV).

2.3.9 The steady state breakdown voltage of air-gaps

In an HVDC system analysis, four possible voltage stresses can occur: a steady state condition, a switching impulse condition, lighting impulse condition and fast transients. The most applicable condition relating to the bird streamer fault, i.e. the steady state condition, was reviewed.

The steady breakdown voltage of rod-plane and rod-rod air-gaps was considered in the literature reviewed. The following is a brief outline of the work that has been performed in this case.

Pigini *et al.* [26] investigated the dielectric strength of air under the application of HVDC.

The results referred to the external insulation in clean conditions (both dry and wet). Both rod-plane and rod-rod gap configurations were considered. It was noted that the flashover voltage was almost proportional to the gap size up to air-gap lengths of 2.5 m.

The average flashover gradient was ≈ 5 $kV.cm^{-1}$ for the rod-rod configuration. In the case of the rod-plane configuration, the negative wet and the positive dry and wet had an average flashover gradient of ≈ 5 $kV.cm^{-1}$.

Knudsen *et al.* [27] investigated the flashover strengths of large air-gaps under HVDC conditions. In these experiments both rod-plane and rod-rod air-gaps were considered. The rods were square cut, with sides 10 mm × 10 mm. The plane was a square with sides 8 m × 8 m.

The rod-rod results produced an average flashover gradient of ≈ 5.5 $kV.cm^{-1}$ (dry conditions). The results for both the negative and positive polarity were very close.

The rod-plane configuration under positive polarity gave rise to an average flashover gradient of 4.8 $kV.cm^{-1}$, while the negative polarity had an average flashover gradient of ≈ 14 $kV.cm^{-1}$ (under dry conditions).

In these experiments it was again noted that the breakdown voltages was proportional to the air-gap length up to 3 m.

Hill *et al.* [28] conducted laboratory tests to determine the HVDC flashover characteristics of air-gaps. Square rod gaps were used, with sides 13 mm × 13 mm. These tests concluded that the HVDC breakdown voltage of air-gaps is a linear function of the gap spacing, for air-gaps up to 1.5 m in length.

The HVDC Reference Book [29] provides an account of the work performed by various authors with regard to the steady state flashover of air-gaps. The report includes summaries of the past work performed on both rod-plane and rod-rod air-gaps. The conclusions reached were that rod-rod and rod-plane air-gaps tend to be a linear function of the air-gap and that neither polarity nor wet or dry conditions affected the steady state flashover of rod-rod air-gaps.

Razevig [30] measured the relationship between the breakdown voltage and the air-gap length for rod-plane air-gaps in the range 0 to 10 cm, with a rod diameter of 4 mm. These tests looked at the effect of the rod tip on the breakdown process. For short air-gaps, the rod tip had an effect on the breakdown voltage. When the rod had a sharp end it resulted in a lower breakdown voltage than in the case where the rod had a hemispherical tip.

2.3.10 The dependence of the breakdown processes on atmospheric conditions

The breakdown voltage of an air-gap is influenced by the ambient atmospheric conditions. By using atmospheric correction factors, an adjustment of the conditions existing during experimental testing can be made [31]. The following section describes the correction procedure adapted from [31].

Standard atmospheric conditions are an air pressure of $b_0 = 1013$ mbar, an air temperature of $t_0 = 20\ ^0C$, and absolute humidity of 11 $g.m^{-3}$.

The atmospheric correction factor (K_t) has two parts, an air density correction factor (k_d), and a humidity correction factor (k_h):

$$K_t = k_h k_d \tag{2.9}$$

The breakdown voltage under standard conditions (U_{corr}) is calculated as:

$$U_{corr} = \frac{U_{bkd}}{K_t} \tag{2.10}$$

where,

U_{bkd} = *breakdown voltage obtained from a test under non – standard conditions*

The air density factor (k_d), depends on the relative air density (δ), and can be expressed by the following equation:

$$k_d = \delta^m \tag{2.11}$$

where,

$$\delta = \frac{b}{b_0} \times \left(\frac{273 + t_0}{273 + t} \right) \tag{2.12}$$

where,
b = ambient air pressure
t = ambient air temperature

The humidity correction factor (k_h) may be expressed as:

$$k_h = k^w \tag{2.13}$$

The exponents, m and w and the value of k are obtained curves provided in [31, 32]. These curves are drawn from experimental work, and their exact values are still under discussion. It must be noted that the exponents m and w depend upon the type of discharge, the breakdown path and the relative air density. Approximate values for m, w, and k can be found from curves contained in [31, 32].

Electra [33] provides a summary of recent work regarding the influence of humidity on non-uniform field air-gap breakdown. Humidity effects on HVDC breakdown indicate that they are dependant upon the length of the air-gap and the geometry of the air-gap. The report highlights the fact that much research work is needed for the humidity effect on air-gaps under DC conditions, thus no humidity coefficient was quoted for larger air-gaps in this report.

Due to the above-mentioned reasons, this dissertation did *not* take the humidity effect (k_h) into consideration in the correction of the experimental results to standard atmospheric conditions.

2.4 Summary of literature findings

2.4.1 Past knowledge gained on bird related fault mechanisms

It is evident that no work has been performed on bird streamer flashovers under HVDC conditions.

From the work performed on the HVAC case, the following key points are noted:

(i) The time of day analysis groups faults caused by either bird streamer or pollution into a specific region.

(ii) Bird deterrents are an effective means of preventing birds from perching on tower tops, but such guards need to be optimally placed in order for them to minimise bird streamer faults.

(iii) No *experimental* work has been done for the HVDC case

(iv) The experimental techniques used by past researchers, and more importantly the characteristics of the artificial bird streamer used, can be used in the HVDC case, and are thus summarised in Table 2.2.

Table 2.2 Characteristics of artificial bird streamers used by previous researchers

Researcher	***Preparation Method***	***Diameter (mm)***	***Conductivity***
Taylor [6]	Saline soaked string	12	25 $mS.cm^{-1}$ and 100 $\mu S.cm^{-1}$
Hoch *et al.* [11]	Specialised experimental apparatus	3	25 $mS.cm^{-1}$
Wang [13]	Specialised experimental apparatus	8	500 $\mu S.cm^{-1}$ to 80 000 $\mu S.cm^{-1}$

It can be noted from Table 2.2, that the conductivities and the diameters of the artificial streamer used by Taylor and Wang show a marginal difference from the ones used by Hoch *et al.*

2.4.2 Electrical discharge phenomena

A systematic literature review process has been undertaken to provide an understanding of the air-gap breakdown processes in both uniform and non-uniform fields.

The literature review has also been applied to provide an understanding of the mechanism of the breakdown process that occurs in a bird streamer fault, and also to explain the *essential* condition that is required for complete air-gap breakdown to occur.

The following paragraphs summarise this.

When the bird streamer is excreted, it falls into the vicinity of an HV tower. This liquid stream is at a grounded potential due to its contact with the grounded tower top. The liquid stream causes a significant enhancement of the electric field in the tower region. The degree of enhancement of the electric field is dependant on the permittivity of the liquid stream. As the distance between the bird streamer tip and the live conductor fitting decreases, streamer inception may occur. The streamer may then cause near bridging of the air-gap between the bird streamer tip and the live conductor fitting. This situation may lead to the formation of an arc,

and this arc may either propagate across the liquid stream or it may disintegrate the liquid stream.

The following *essential* condition must be met in order for complete air-gap breakdown to occur:

(i) The liquid stream must have a large enough permittivity to cause a significant enhancement of the electric field in the tower region.

The aim of this dissertation is to find a horizontal distance (protected zone) on an HVDC tower top, in order to move a bird, and thus a bird streamer away from the centre of the tower. In doing this the characteristics of the bird streamer will be studied. The protected zone length will in essence, result in a reduction of the enhancement of the electric field in the tower area, thus decreasing the likelihood of electrical streamer inception. This can be seen in Figure 2.9. (The protected zone will in effect, increase the air insulation between the bird streamer tip and the live conductor fitting).

2.5 Conclusion

Chapter Two has presented a review of the literature relevant to the bird streamer phenomenon, and in doing so, has proposed a model for the bird streamer mechanism. This understanding has led to a solution method which is used to minimise the occurrence of bird streamer faults, i.e. the protected zone length.

The following chapter deals with the experimental apparatus and procedure, which was needed for the experiments.

3 EXPERIMENTAL APPARATUS AND PROCEDURE

Experimental work has been performed to provide an understanding of the insulation strength of air-gaps (stressed under both HVDC and HVAC) under a bird streamer intrusion (under *static* conditions), and in doing so, has led to calculation of the protected zone on an HVDC and HVAC tower top.

This Chapter presents a description of the experimental facilities, design, layout and procedure.

A description of the geometric configuration that was modelled in QuickField™ will be presented.

3.1 Laboratory facilities

3.1.1 HVDC generator

The HVDC laboratory situated at the University of KwaZulu-Natal has a two-stage Walton-Cockcroft type HVDC generator. A schematic drawing of the generator circuit, together with a simplified test circuit is shown in Figure 3.1. The generator has a maximum output voltage of +500 kV and -540 kV and a continuous output current of 7.5 mA. The ripple factor at maximum load is less that 3% [34].

The maximum voltage attainable in the laboratory is significantly reduced due to height restrictions. The maximum voltage output is in the region of 230 kV. AC power is supplied to a step up transformer via a voltage regulator, which varies the input voltage between 0 kV and 100 kV. The Walton-Cockcroft circuit then converts the AC voltage to HVDC. The output voltage is measured by means of a potential divider circuit, shown in Figure 3.1.

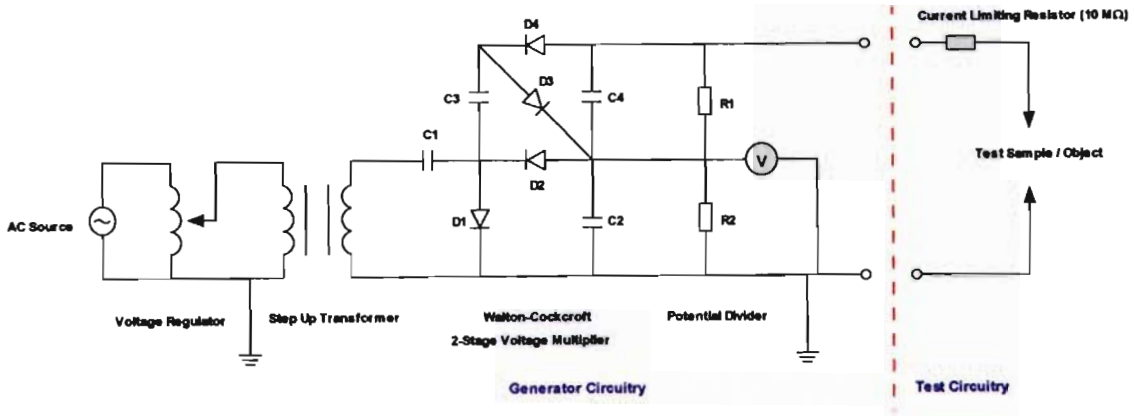

Note: C_1 = 100 000 pF, $C_2 = C_3 = C_4$ = 50 000 pF, $R_1 = R_2$ = 600 MΩ

Figure 3.1 Schematic representation of the HVDC generator and the simplified test circuit, *(reproduced from [34])*

3.1.2 Test tower design

In order to understand the bird streamer air-gap breakdown phenomenon, laboratory experiments on a model transmission tower with V-String and I-String insulator configurations were carried out.

Two key factors were taken into account during the design of the model transmission tower:

(i) Space constraints in the laboratory.

(ii) Voltage output of the HVDC generator and hence air-gap clearances.

These were considered to avoid flashover to the grounded tower.

From the literature reviewed [26-30], a reasonable assumption for the average flashover gradient under both negative and positive polarities under HVDC conditions was chosen to be 500 kV.m^{-1}. Using this flashover gradient, the required air-gap length to prevent flashover from occurring at a specific applied voltage level can be calculated as follows:

$$Clearance\ Distance = \frac{V_{HVDC}}{E_{av}} \qquad (3.1)$$

where

E_{av} = *average flashover gradient*

V_{HVDC} = *applied voltage*

Applying a value of 230 kV (the maximum allowable output voltage of the HVDC generator) as the applied voltage (V_{HVDC}) and a value of 500 $kV.m^{-1}$ for the average flashover gradient (E_{av}) into Equation (3.1), results in a clearance distance of 0.46 m.

The tower dimensions were then selected using the calculated clearance distance and the dimensions of the available working space in the HVDC laboratory, resulting in a length greater than 0.46 m. This meant that the tower could be used at higher voltage levels, when a larger power supply becomes available. The outlay of the tower is shown in Figure 3.2.

The structure proved to be a key component in the experimental testing phase, as it was adjustable both vertically and horizontally (shown in Figure 3.2). This meant that insulators could be placed under test, using *either* a V-String or I-String configuration (shown in Figure 3.2).

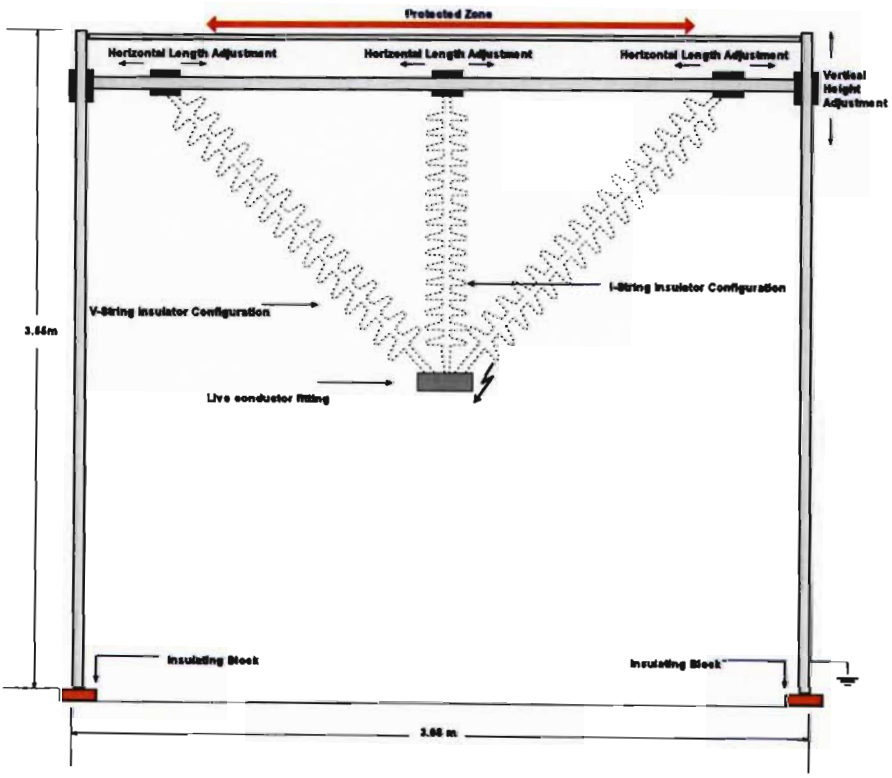

Figure 3.2 Model HVDC transmission tower, (including insulator configurations)

3.2 Experimental apparatus

The insulators used in the experiments were the 132 kV AC silicone rubber type. Further details of the insulator are provided in Appendix B.

Chapter Two outlined the various methods of preparing an artificial bird streamer, from these methods, the most applicable were chosen for the purposes of this research. It was initially decided to use a brass rod as an artificial streamer, and later to use a string soaked in a saline solution as the artificial streamer. These two methods allowed for controlled lengths of air-gap/streamer lengths to be generated, which is not possible when using a liquid streamer.

Two saline solutions were used, enabling two different streamer conductivities to be prepared. The first solution had a conductivity of 10 $\mu S.cm^{-1}$ and the second 10 000 $\mu S.cm^{-1}$.

3.2.1 Rod-Plane and rod-rod air-gaps

The air-gap between the simulated bird streamer and the live conductor fitting was assumed to be alike to a rod-plane air-gap configuration (indicated in Figure 3.3). This was explained through the experimental results provided in Chapter Four.

3.2.1.1 Brass Rod – Live conductor fitting (HVDC)

This experiment was performed to determine the air-gap breakdown characteristics between an artificial bird streamer (brass rod) and a live conductor fitting, and did not take into account the effect of insulator strings.

It is known that the breakdown voltage of a typical rod-plane air-gap (short air-gap) is dependant on the tip profile. A conical tip produces the lower breakdown voltage compared to flat and hemispherical tip profiles as discussed in section 2.3.9 [30], but as the length of the air-gap increases, the dependence on the tip profile decreases, due to space charge surrounding the electrodes. A conical rod tip profile was chosen for the artificial bird streamer, based on the fact that in short air gaps, it would provide the lowest possible breakdown voltage. The rod diameter was chosen to be 10 mm; this value was in the range of diameters used by previous researchers studying this phenomenon in the HVAC case (outlined in Table 2.2). Intuitively, a round rod was chosen over a square type. This was done in order to generate a streamer similar to that of one occurring naturally.

The test layout is shown in Figure 3.3. The live electrode was supported using an insulating string (for simplicity, the string is not shown in Figure 3.3), thus ensuring insulation between the energised live conductor fitting and the grounded tower.

Figure 3.3 indicates three lengths, an air-gap length (D), the bird streamer length (L), and the total length (T), where, T = L + D.

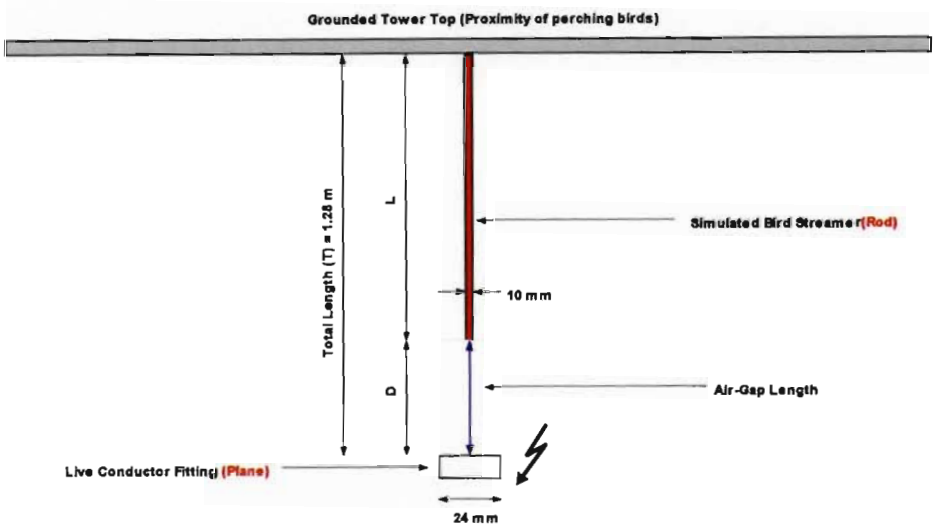

Figure 3.3 Layout of the rod-plane experiment, air-gap breakdown between the brass rod and the live conductor fitting

3.2.1.2 Saline string - Live conductor fitting (HVDC)

This experiment was performed to determine the air-gap breakdown characteristics between an artificial bird streamer (saline solution soaked string) tip and the live conductor fitting, for the purpose of a comparison between air-gap breakdown strengths for two different streamer conductivities. This experiment did not take into account the effect of insulator strings.

The experimental layout is shown in Figure 3.4. The live electrode was supported using an insulating string.

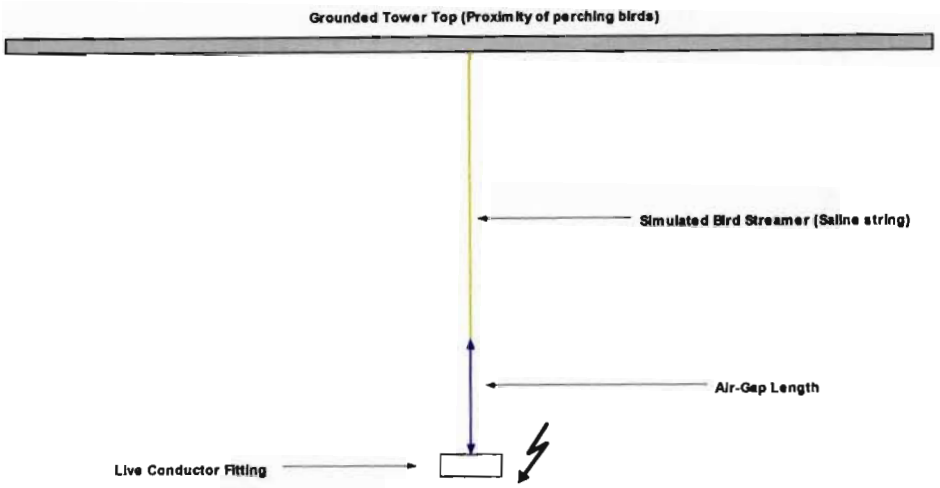

Figure 3.4 Layout of the rod-plane experiment, air-gap breakdown between the soaked string and the live conductor fitting

3.2.1.3 Rod-Plane (short air-gaps) experimental setup (HVDC)

This experiment was performed to validate the results obtained from the air-gap between the brass rod and the live conductor fitting of section 3.2.1.1. The arrangement comprised a rod with a diameter of 15 mm, and a plane with a diameter of 160 mm, the layout of which is shown in Figure 3.5. High voltage DC was supplied to the rod and in the subsequent experiment, to the plane.

These experiments were performed under both negative and positive polarity. A total of four configurations were used in this experiment (i.e. two configurations for each polarity).

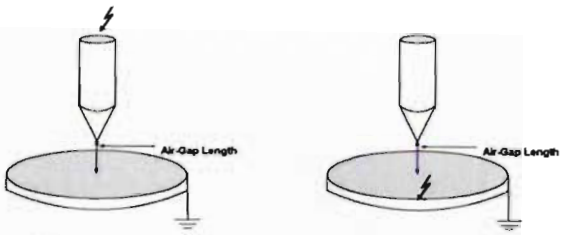

(a) Application of HVDC to the rod **(b)** Application of HVDC to the plane

Figure 3.5 Layout of the rod-plane arrangement experiment for small air-gaps

3.2.1.4 Rod-Plane and rod-rod air-gaps (HVDC)

This experiment was performed to provide a comparison of breakdown voltages between rod-plane and rod-rod electrode configurations.

The rod-plane configuration comprised a rod with a diameter of 10 mm, and a plane with a diameter of 1000 mm, and the rod-rod configuration comprised a rod with a diameter of 10 mm.

The experimental layout is shown in Figure 3.6. These tests were performed under both negative and positive polarity. In the rod-plane configuration, HVDC was applied to the plane.

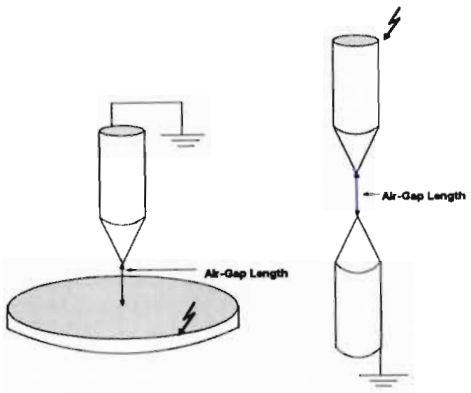

Figure 3.6 Layout of the rod-plane arrangement experiment for small air-gaps

3.2.2 V-String insulator configuration

These experiments were performed in order to find the length of the protected zone on an HVDC tower top.

These experiments considered two possible variations to the intrusion of the bird streamer: a lateral intrusion and a horizontal intrusion (shown in Figures 3.7 and 3.8 respectively).

These experiments were *also* performed under HVAC conditions.

3.2.2.1 Lateral bird steamer intrusion

This experiment was performed in order to find the length of the protected zone on an HVDC tower top. The experiment was performed with a corona ring, placed in a conventional position below the bottom of the insulator string (shown in Figures 3.7).

The bird streamer was inserted from the tower top, whereby air-gap breakdown occurred laterally, between the streamer tip and the corona ring, as shown in Figure 3.7.

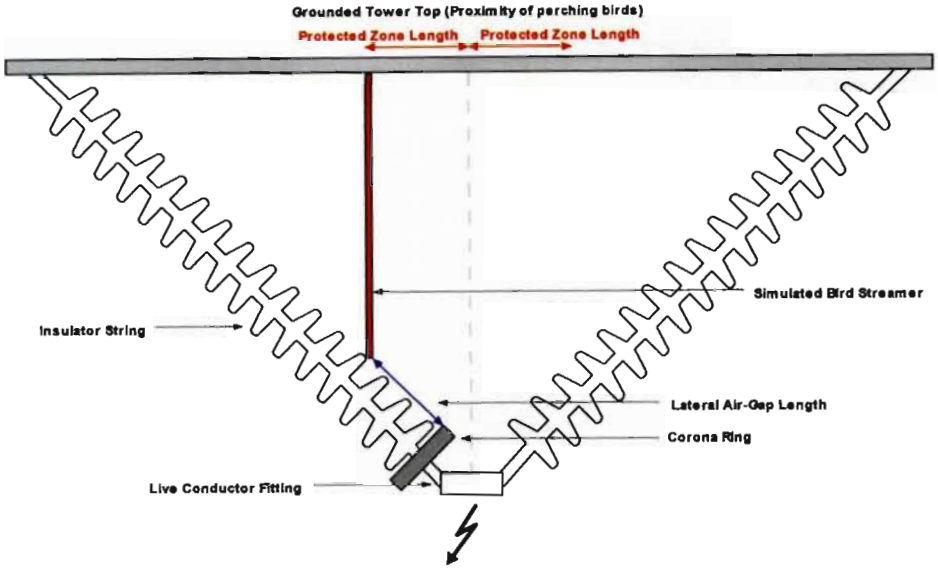

Figure 3.7 Layout of the V-String insulator experiment, *lateral* air-gap breakdown between the brass rod and the live conductor fitting

3.2.2.2 Horizontal bird streamer intrusion

This experiment looked at the possibility of horizontal air-gap breakdown between the brass rod and the corona ring, as shown in Figure 3.8. The experiment was performed with the inclusion of a corona ring.

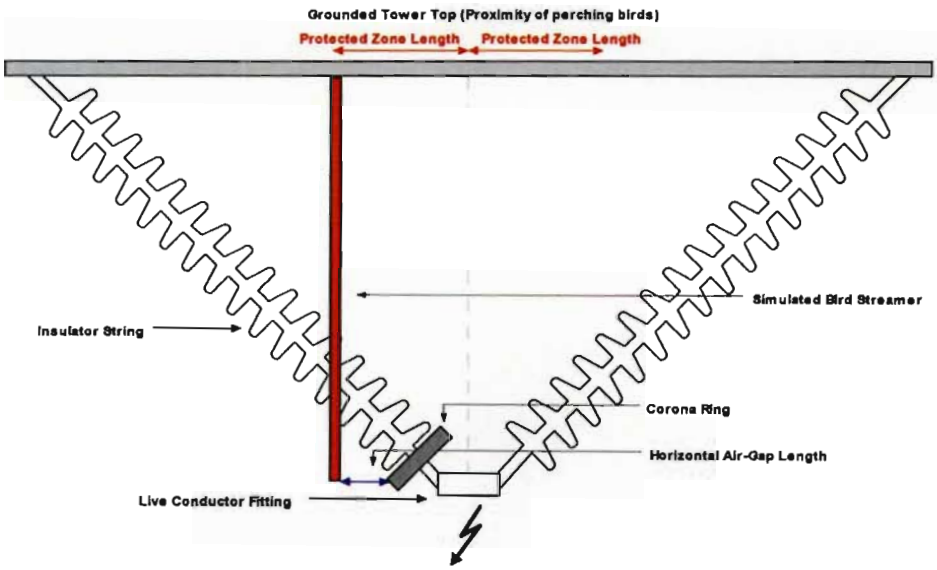

Figure 3.8 Layout of the V-String insulator experiment, *horizontal* air-gap breakdown between brass the rod and the live conductor fitting

3.2.3 I-String insulator configuration

The aim of these experiments was to find a protected zone on an HVDC tower top. This experiment looked at horizontal air-gap breakdown. The experimental setup is shown in Figure 3.9.

The experiment was performed with and without a corona ring.

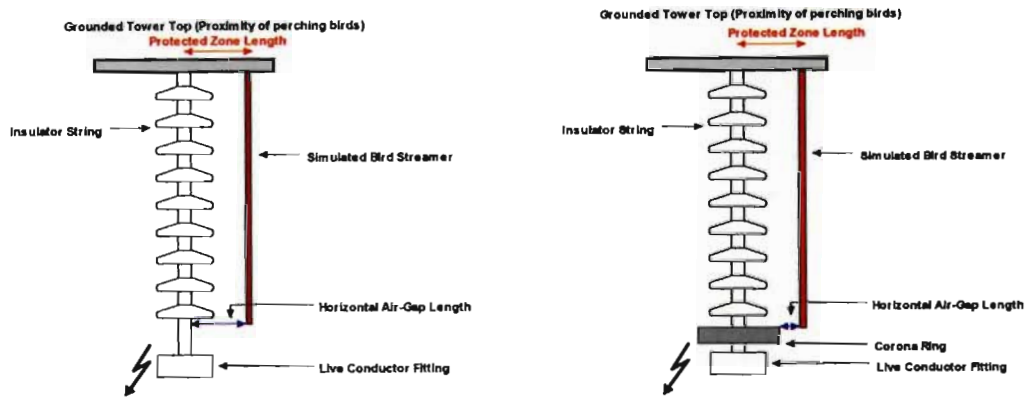

(a) *Without corona Ring* **(b)** *With corona Ring*

Figure 3.9 Layout of the I-String insulator experiment, *horizontal* air-gap breakdown between the brass rod and the live conductor fitting

3.2.4 Floating bird streamer

In this dissertation, it was assumed that the bird streamer remained in contact with the grounded tower top during its decent from the tower top, up until breakdown occurred.

A possible alternative to this situation was considered, whereby the streamer did not remain in contact with the tower top after descent, but became a floating streamer. This scenario seemed to be rather interesting for further work, though saying that, one set of experiments was performed in order to gain some insight on this concept.

In these experiments, the brass rod (with a fixed length) was located at various positions away from the grounded tower top. Figure 3.10, indicates two air-gap paths, D_1 and D_2. D_1 was varied from 0 to $D_2 = 0$. The total length (T) remained fixed at 1 m. The live conductor fitting was again held in position by an insulating string. The negative polarity case was looked at only, where the length of the artificial streamer (L) was 0.65 m.

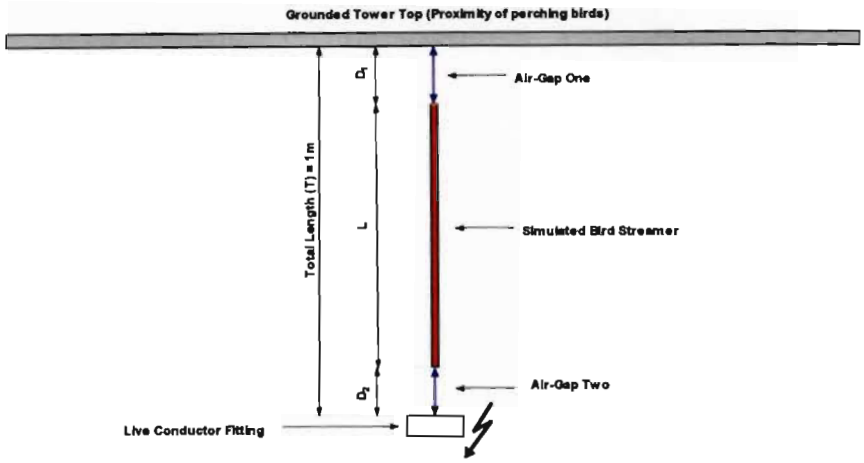

Figure 3.10 Layout of the floating bird streamer experiment, brass rod-live conductor fitting with a double air-gap

3.3 Experimental procedure

The temperature, humidity and pressure were all noted at the start of the experiments. The results were then corrected to standard temperature and pressure (STP), as required by the IEC specifications [31]. The breakdown voltage was taken as the mean of 6 consecutive breakdowns.

In the experiments, the air-gap path was fixed at a pre-determined length (D), while the length of the bird streamer (L) varied. The total gap lengths (T) were 1.28 m and 1.52 m for the V-String and I-String configurations respectively, whereas T in the case of the floating bird streamer was 1 m in length.

The bird streamer was placed in the positions as discussed in the previous sections.

The live conductor fitting was then energised, and the applied voltage was increased until breakdown occurred. The breakdown voltage and the air-gap length were recorded for each air-gap length under test.

3.4 The finite element method (FEM)

The electric field distribution between the bird streamer tip and the live conductor fitting was modelled and analysed using an FEM package called QuickField™. A more accurate means of determining the electric field intensity can be found through measurement using a DC field meter.

Field meters can take into account, the polarity effect under HVDC conditions, and hence space charge distribution, something that cannot be accomplished with the FEM package QuickField™. Access to a field meter was not possible, and thus QuickField™ was used to provide the analysis.

QuickField™ was used to examine the electric field distribution in both a rod-plane and a rod-rod electrode configuration, based on the breakdown characteristics of the simulated bird streamer. The maximum electric field in the gap was examined for different air-gap distances and rod-plane electrode geometries in order to explain the discharge phenomena associated with the bird streamer air-gap breakdown process.

These simulations were thus performed in order to examine two processes:

(i) To show how the maximum electric field intensity in an air-gap increases as the simulated bird streamer is introduced to the air-gap, thus satisfying the streamer propagation criteria laid out in section 2.3.5.

(ii) To show how the effect of a rod-plane electrode configuration geometry affects the electric field intensity in an air-gap, thus affecting the air-gap breakdown voltage.

3.4.1 Variation in the air-gap length

In this set of simulations, a rod-plane electrode configuration was modelled. The air-gap length ranged from 100 mm to 300 mm. A layout of the rod-plane configuration modelled is shown in Figure 3.11.

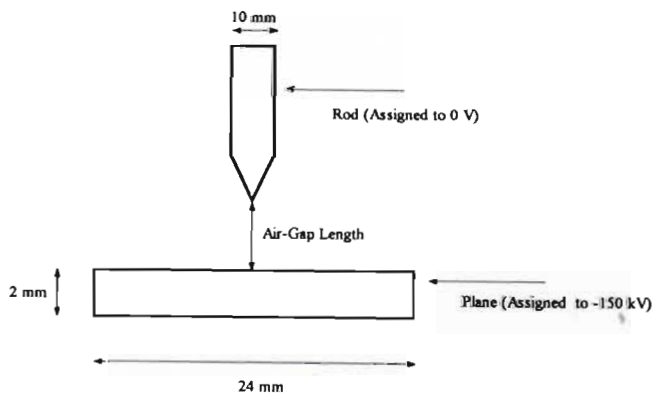

Figure 3.11 Rod-Plane electrode configuration (circular cross-section)

The geometry was modelled under the *axisymmetric* class. A QuickField™ geometric model of the rod-plane arrangement is shown in Figure 3.12.

In the simulations, the rod was assigned a voltage 0 V, while the plane was assigned a voltage of -150 kV.

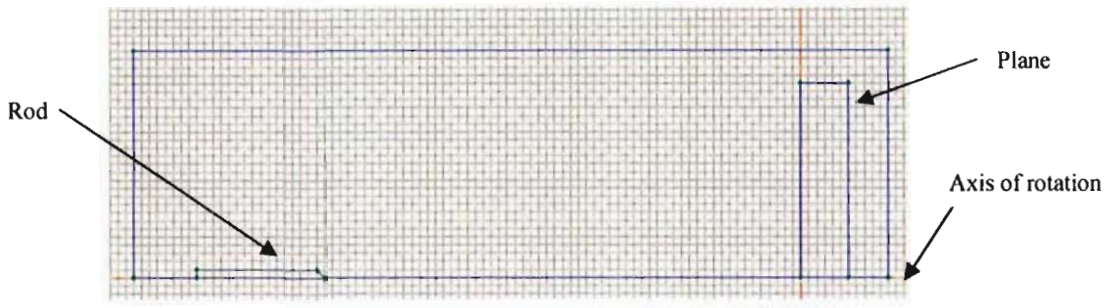

Figure 3.12 QuickField™ geometric model of the rod-plane electrode configuration

3.4.2 Variation in the rod-plane electrode geometry

In this set of simulations, a rod-plane electrode configuration was modelled. The rod was set to 0 V and the plane was set to an arbitrary voltage of -44 kV.

In this model, the rod diameter was 10 mm and the plane diameter ranged from 240 mm to 10 mm. The geometry was modelled under the *axisymmetric* class. A QuickField™ geometric model of the rod-plane electrode configuration is shown in Figure 3.13.

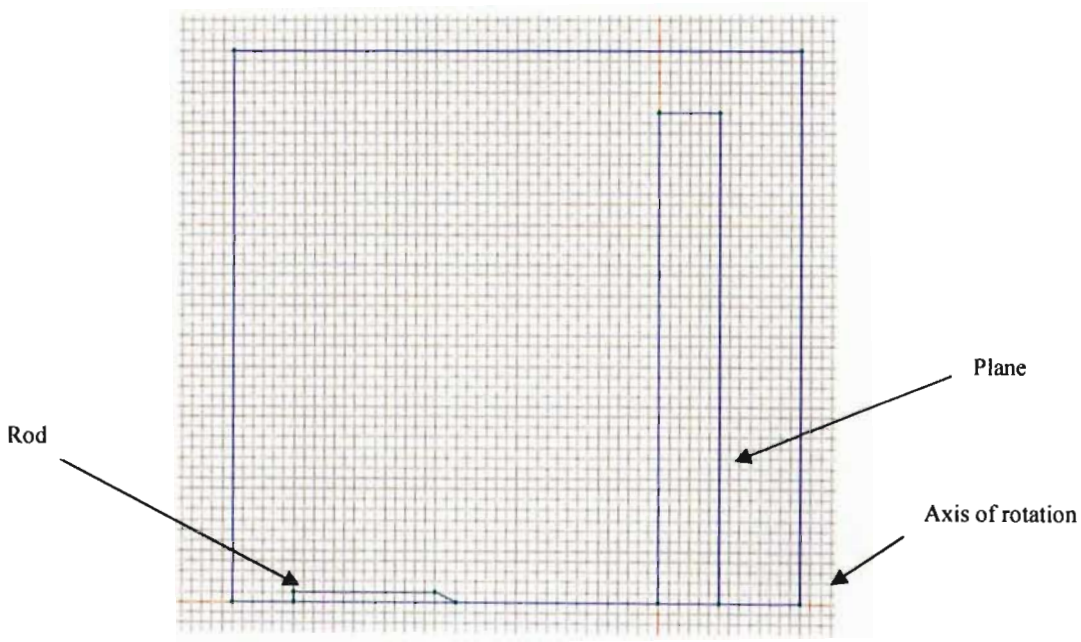

Figure 3.13 QuickField™ axisymmetric geometric model of the rod-plane electrode configuration

3.5 Conclusion

This chapter has introduced the experimental apparatus and procedure that has been used in this dissertation. The various field simulation models have also been presented for the various insulator configurations.

Chapter four will present the experimental and field simulation results, followed by a discussion and application of the results, with relevance to the calculation of the protected zone.

4 RESULTS AND DISCUSSION FOR AIR-GAPS UNDER NON-UNIFORM ELECTRIC FIELDS

This chapter presents the experimental results for air-gap breakdown under non-uniform HVDC and HVAC stresses (the experimental set-up of which was detailed in Chapter 3). These results, together with previous HVAC work performed by Taylor [6] and Hoch *et al.* [11], will be compared and discussed.

Finally, the FEM results are presented, with relevance to the change in the electric field intensity as the simulated bird streamer approaches the live conductor fitting. The electric field simulation proved to be crucial in understanding the outcomes of the experiments conducted.

4.1 Results and discussion of experimental work

4.1.1 Brass Rod-Live conductor fitting (HVDC)

This experiment was done in order to determine the insulation strength of a variable air-gap between a simulated bird streamer (brass rod and a string soaked in a saline solution) and a live conductor fitting.

Figure 4.1 shows the relationship between the breakdown voltage and the air-gap length. In each case the rod is grounded, and HVDC was applied to the plane.

Figure 4.1(a) contains the results under negative polarity, while Figure 4.1(b) contains the results under positive polarity.

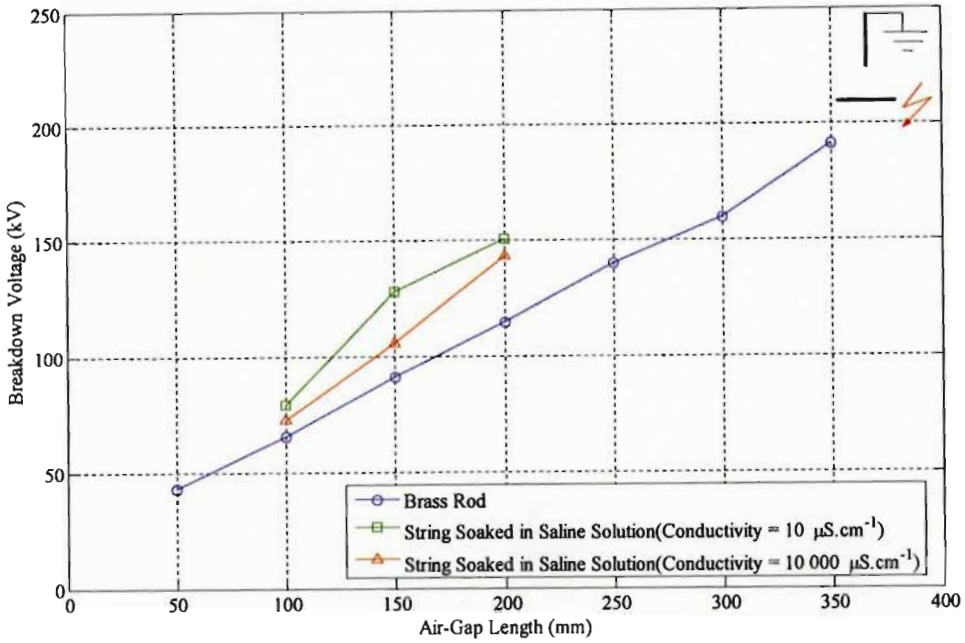

(a) Negative HVDC

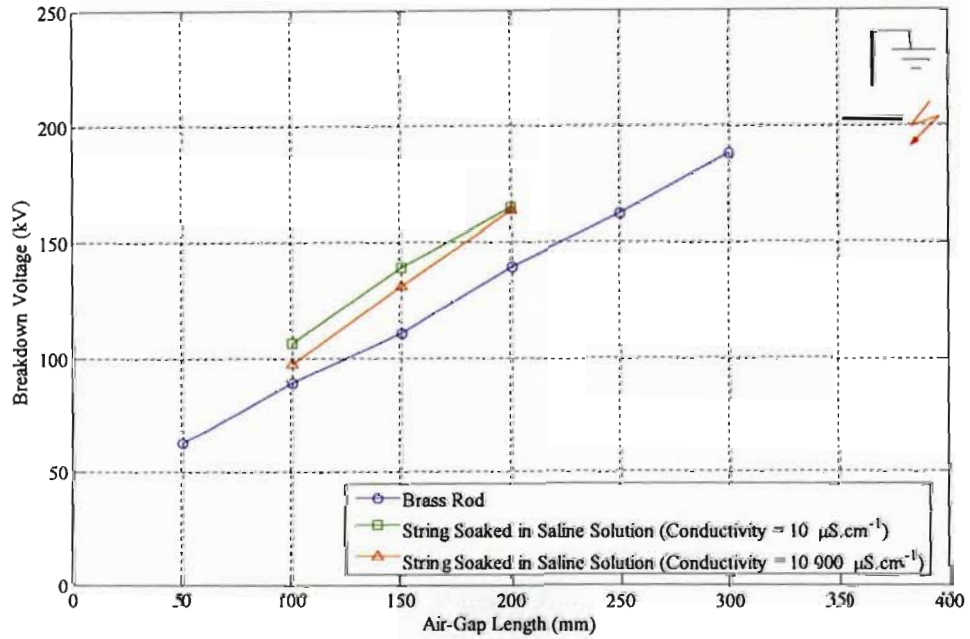

(b) Positive HVDC

Figure 4.1 Rod-Plane experiment, breakdown voltage as a function of air-gap length

Analysis of Figure 4.1 indicates that the breakdown voltages are greater under positive polarity than negative polarity. The increase in breakdown voltages under positive polarity is on average 28% greater than under negative polarity.

An assumption was arrived at in Chapter Two, namely that the air-gap between the bird streamer tip and the live conductor fitting resembled that of a rod-plane electrode arrangement. Based on the literature reviewed on the rod-plane and rod-rod electrode configurations, ***two*** deviations are noted when comparing the current experimental results to the ones in [26-30],

(i) The breakdown voltage under a negative polarity rod and a grounded plane is greater than under a positive polarity rod and a grounded plane [26-30] (i.e. a higher gradient is noted under negative polarity than under positive polarity. However, this is not the case in the current experimental results. A key point noted from the experiments of [26-30], was that HVDC was applied to the rod (i.e. the plane was grounded) and *not* to the plane. In the present experiments, the converse was done, whereby the plane was energised with HVDC and the rod was grounded. The results seem reasonable, on the basis of the discussion of section 2.3.7. This is further verified in sections 4.1.2 and 4.2.1.

(ii) The results obtained for the air-gap between the grounded brass rod and the negative polarity live conductor fitting in dry conditions are in agreement with that of [26, 27, and 29] (subject to the reversal of polarities). The results for the positive polarity show a deviation to the results obtained in [26, 27 and 29] under the rod-plane electrode configuration. An explanation for this is that the plane in the rod-plane configuration used in [16, 18] and the plane used in this dissertation have different lengths. This would mean that as the length of the plane decreases, the electric field lines become concentrated around a smaller length, thus affecting the air-gap breakdown characteristics. Further explanation of this occurrence will be discussed in sections 4.1.3 and 4.2.2.

Figure 4.1 shows a small variation between the results obtained for the soaked strings of two different conductivities.

This small variation means that for a streamer conductivity of between 10 μS and 10 000 μS, the difference between breakdown voltages is marginal.

The breakdown voltage for the 10 000 μS saline soaked string was on average 18% greater than the brass rod under negative polarity, while the 10 000 μS saline soaked string was on average 16% greater than the brass rod under positive polarity. This increase in breakdown strength seems reasonable due to the higher impedance of the soaked string compared to the brass rod. For a comparison of the breakdown voltage between a brass rod and soaked string (with a conductivity of 10 000 μS), the wet string has higher breakdown voltage strength of ≈ 20%.

4.1.2 Rod-Plane (short air-gaps, HVDC)

This experiment was performed in order to validate the breakdown voltage variation resulting in the application of HV from the plane to the rod, as discussed in section 4.1.1.

Figure 4.2 shows the relationship between the breakdown voltage and the air-gap length for gap lengths in the range 10 mm to 60 mm.

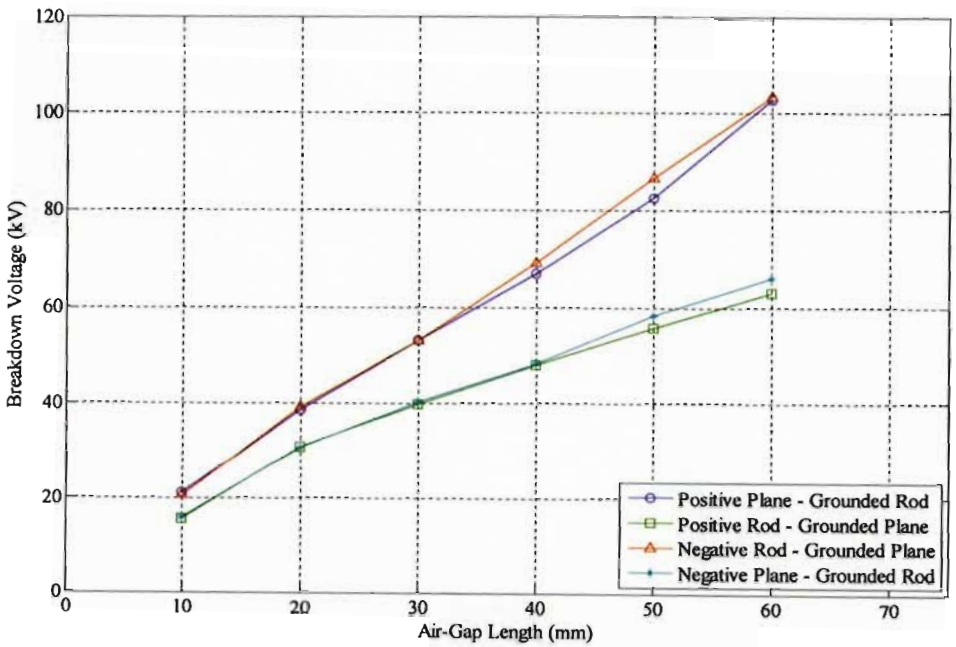

Figure 4.2 Rod-Plane experiment (short air-gaps), negative and positive HVDC, breakdown voltage as a function of air-gap length

Analysis of Figure 4.2 indicates that when the rod is positive with respect to the plane, the result is a lower breakdown voltage than when the rod is negative with respect to the plane. The reasoning behind this stems from the streamer propagation criteria discussed in section 2.3.5.

This implies that a lower field at the tip of the streamer is required for positive streamer propagation than for negative streamer propagation.

These results were essential in validating the results of Figure 4.1, and agree well with the discussion of section 2.3.7.

The results obtained in Figure 4.3 are in good agreement with that of Razevig [30].

4.1.3 Rod-Plane and rod-rod air-gaps (HVDC)

This experiment was performed in order to describe the breakdown voltage variation between the negative and positive polarity, as discussed in section 4.1.1. This experiment was also used as means of assessing the results obtained in section 4.1.1.

Figure 4.3 shows the relationship between the breakdown voltage and the air-gap length for rod-plane and rod-rod electrode configurations.

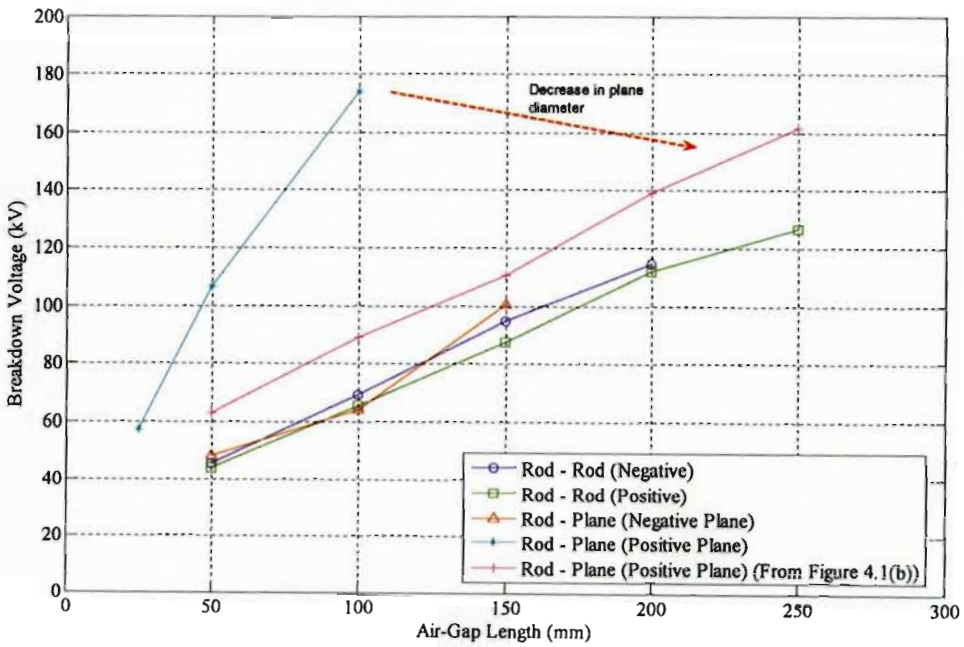

Figure 4.3 Rod-Plane and Rod-Rod experiments, negative and positive HVDC, breakdown voltage as a function of air-gap length

Analysis of Figure 4.3 with reference to the rod-plane arrangement indicates that the average flashover gradient is $\approx$ 14.2 kV.cm^{-1} for the positive plane, and $\approx$ 5.1 kV.cm^{-1} for the negative plane. The rod-rod results of Figure 4.3 show an average flashover gradient of $\approx$ 4.3 kV.cm^{-1} for both the negative and positive polarities.

The results of Figure 4.3 are in good agreement with that of [26, 27].

An explanation for the variation in results for the rod-plane arrangement shown in Figure 4.1, and that of Figure 4.3 are attributed to the diameter of the plane in each case in relation to the diameter of the rod. As the diameter of the plane decreases, the electrode configuration tends to that of a rod-rod configuration. The air-gap between the bird streamer and the live conductor fitting constitutes an intermediate electrode configuration. This can be seen in Figure 4.3, where the results of the brass rod bird streamer (from Figure 4.1(b)) are used to depict this intermediate property.

A key point to note is that the rod-plane electrode configuration is dependant on the effect of polarity (which is observed in the current experimental results), while the rod-rod electrode configuration is not significantly dependant on the effect of polarity [29].

On the basis of this experimental work, the configuration between the bird streamer tip and the live conductor fitting can be considered to be a rod-plane. This reasoning is mainly due to the significant difference in breakdown voltages between the negative and positive HVDC applications.

Further work was performed to model the electric field intensity variation between the rod and the plane in a typical rod-plane configuration as the cross sectional length of the plane is varied. This is discussed in section 4.2.2.

4.1.4 V-String insulator configuration (HVDC)

4.1.4.1 Lateral bird streamer intrusion

This experiment was performed in order find the length of the protected zone on an HVDC tower top. The orientation of the bird streamer was such that air-gap breakdown occurred laterally, between the streamer tip and the corona ring.

Figure 4.4 shows the relationship between the breakdown voltage and the air-gap length for the lateral streamer intrusion. Figure 4.4(a) contains the results under negative polarity, while Figure 4.4(b) contains the results under positive polarity. These results are compared to the rod-plane results of sub-chapter 4.1.1 (depicted by the green curves in Figure 4.4).

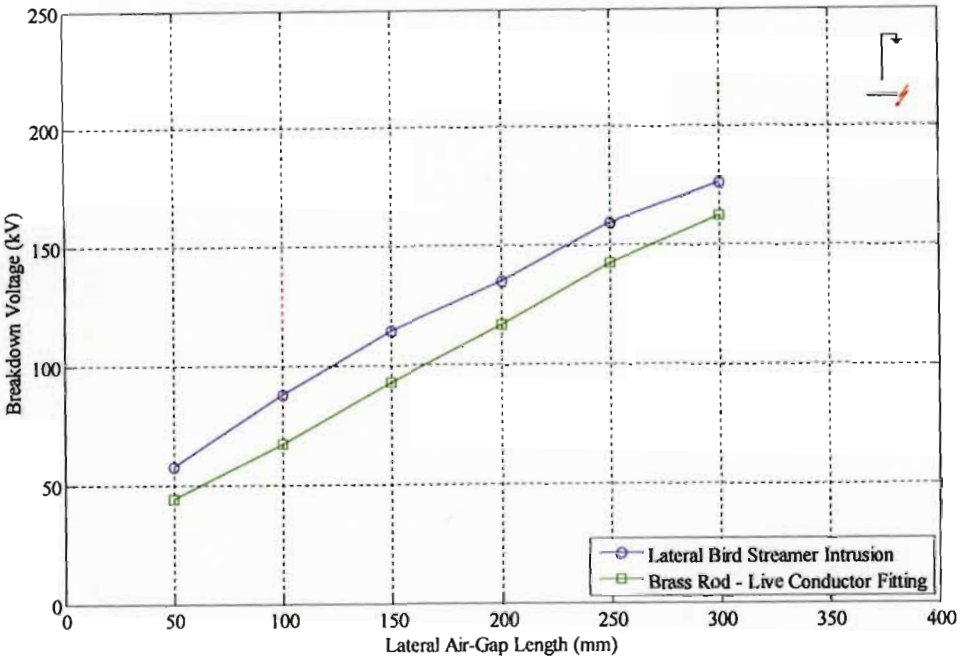

(a) Negative HVDC

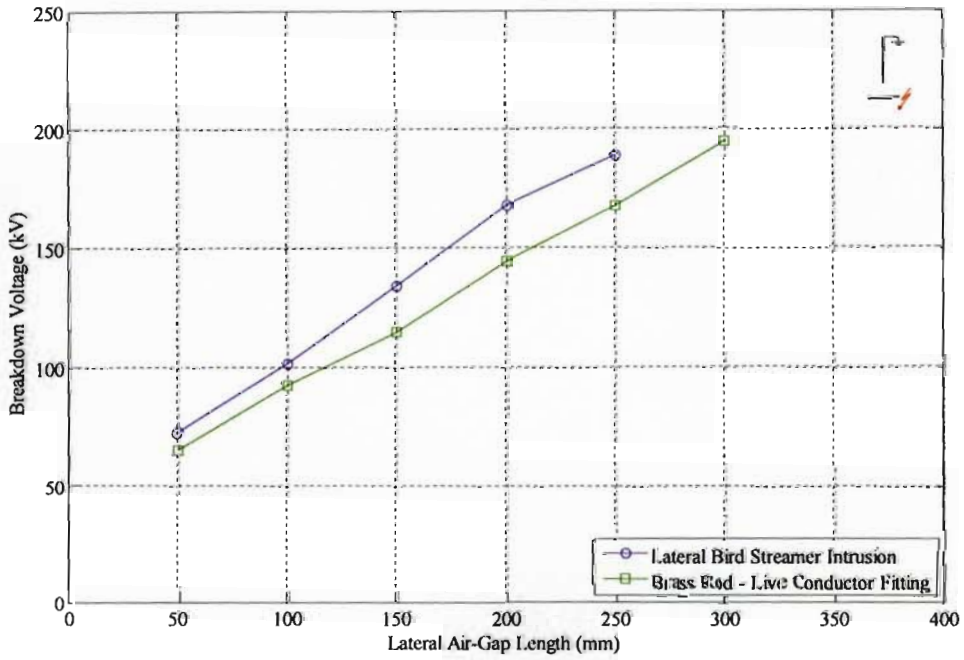

(b) Positive HVDC

Figure 4.4 V-String experiment, breakdown voltage as a function lateral air-gap length

Analysis of Figure 4.4 indicates that the breakdown voltages for the lateral streamer intrusion are greater than the rod-plane arrangement (an average increase of 22% and 20% for the negative and positive polarity respectively).

This increase could lead to the possibility that the presence of the insulators may play a role in the air-gap breakdown process.

4.1.4.2 Horizontal bird streamer intrusion

This experiment was performed in order to find the length of the protected zone on an HVDC tower top. The orientation of the bird streamer was such that air-gap breakdown occurred horizontally, between the streamer tip and the corona ring.

Figure 4.5 shows the relationship between the breakdown voltage and the air-gap length for the horizontal streamer intrusion. Figure 4.5(a) contains the results under negative polarity, while Figure 4.5(b) contains the results under positive polarity. These results are compared to the rod-plane results of section 4.1.1.

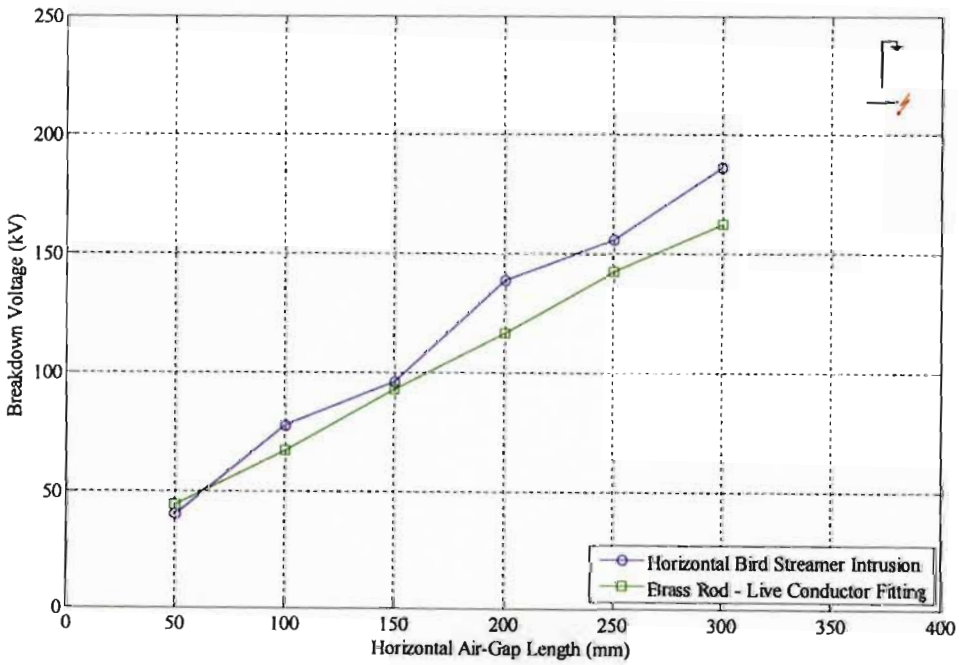

(a) Negative HVDC

Figure 4.5 *V*-String experiment, breakdown voltage as a function of horizontal air-gap

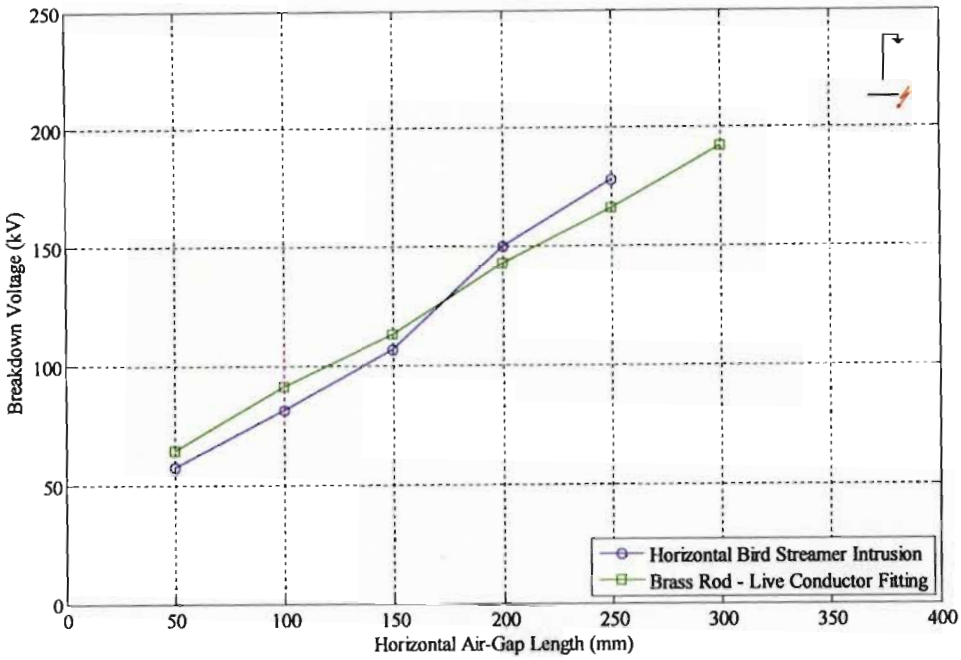

(b) Positive HVDC

Figure 4.5 V-String experiment, breakdown voltage as a function of horizontal air-gap length

Analysis of Figure 4.5 indicates that the breakdown voltages for the horizontal streamer intrusion are similar to the rod-plane configuration.

4.1.5 I-String insulator configuration (HVDC)

This experiment was performed in order find the length of the protected zone on an HVDC tower top for an I-String insulator configuration. The orientation of the bird steamer was such that air-gap breakdown occurred between the corona ring and the bottom of insulator string for the case with and without a corona ring respectively.

Figure 4.6 shows the relationship between the breakdown voltage and the air-gap length, for air-gap breakdown in the horizontal plane, for both the artificial bird streamers. Figure 4.6(a) contains the results under negative polarity, while Figure 4.6(b) contains the results under positive polarity. These results are compared with the rod-plane results of section 4.1.1.

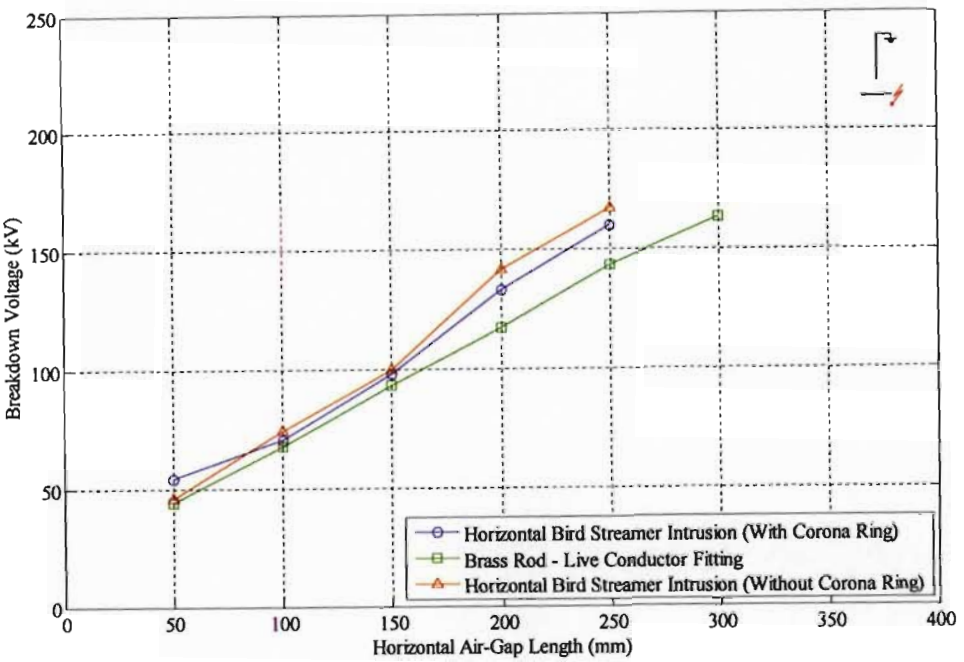

(a) Negative HVDC

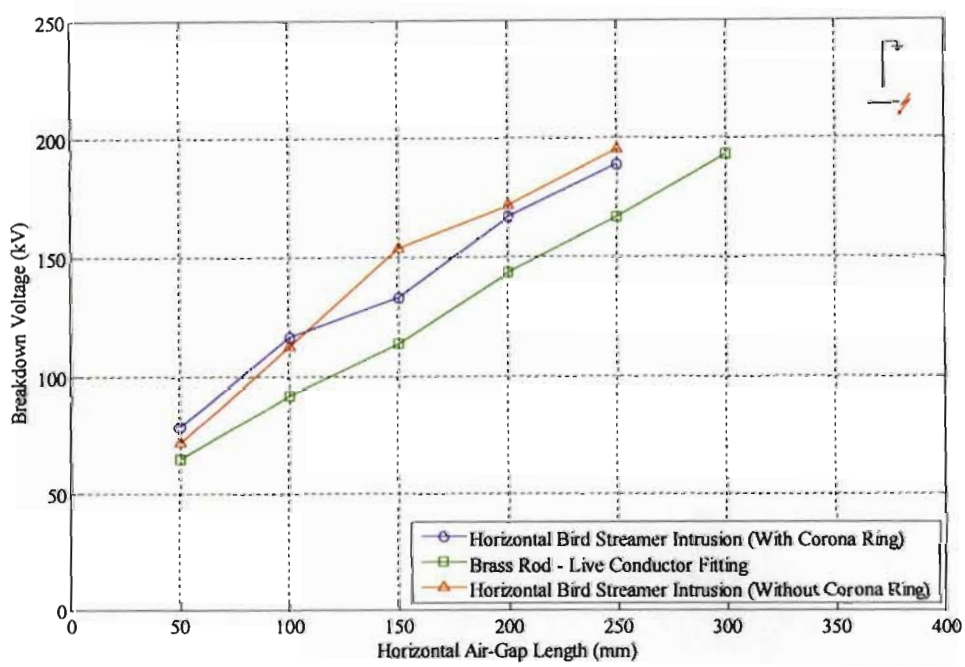

(b) Positive HVDC

Figure 4.6 I-String experiment, breakdown voltage as function of horizontal air-gap length

Analysis of Figures 4.6 indicates that the voltage breakdown levels for the horizontal streamer intrusion are greater than the rod-plane configuration (an average increase of 14% and 23% for

the negative positive polarity respectively with the corona ring, and an average increase of 15% and 25% for the negative positive polarity respectively without the corona ring).

4.1.6 Floating bird streamer (HVDC)

(The lengths L, D_1 and D_2 referred in this section, are indicated in Figure 3.10 of Chapter 3)

This section discusses the floating bird streamer under the negative polarity, because of its lower breakdown strength. During these experiments, two air-gap breakdown processes occurred almost simultaneously. The first between, the tower top and the back end of the bird streamer (air-gap D_1), and the second, between the bird streamer tip and the live conductor fitting (air-gap D_2.)

4.1.6.1 Negative polarity

Figure 4.7 shows the relationship between the breakdown voltage and the air-gap length (D_1), for the floating bird streamer under negative polarity.

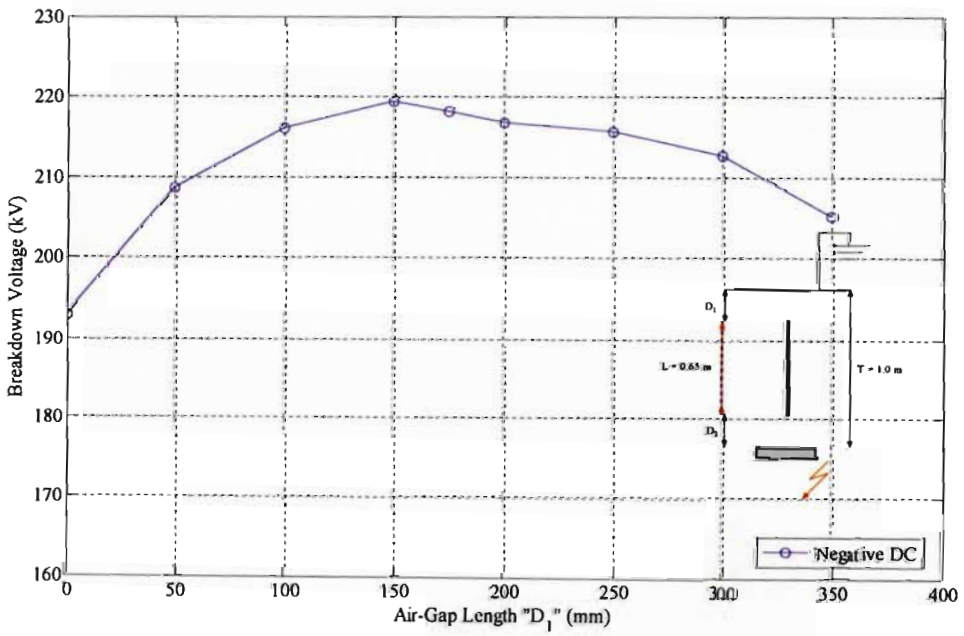

Figure 4.7 Floating bird streamer experiment, negative HVDC, breakdown voltage as a function of air-gap length

NB: ***In this experiment the length of the simulated bird streamer (L) = 0.65 m***

Analysis of Figure 4.7 leads to the following statements:

(i) The breakdown strength is at a maximum in the region where $D_1 \approx D_2$.

(ii) The breakdown voltage when $D_2 = 0$ is greater than the breakdown voltage when $D_1 = 0$ (an increase of 6%). This is attributed to the change from a grounded rod to an energised rod.

(iii) The breakdown voltage near the centre (i.e. $D_1 \approx D_2$) is 14% and 7% greater than when $D_1 = 0$, and when $D_2 = 0$ respectively.

4.1.6 V-String insulator configuration, lateral and horizontal air-gap breakdown (HVAC)

These experiments were performed in order to provide a comparison with the experimental procedure used in this dissertation to that of previous research work performed by Taylor [10] and Hoch *et al.* [11]

Figure 4.8 shows the V-String results produced by Taylor and the results produced by the present author. These results are for both lateral and horizontal air-gap breakdown.

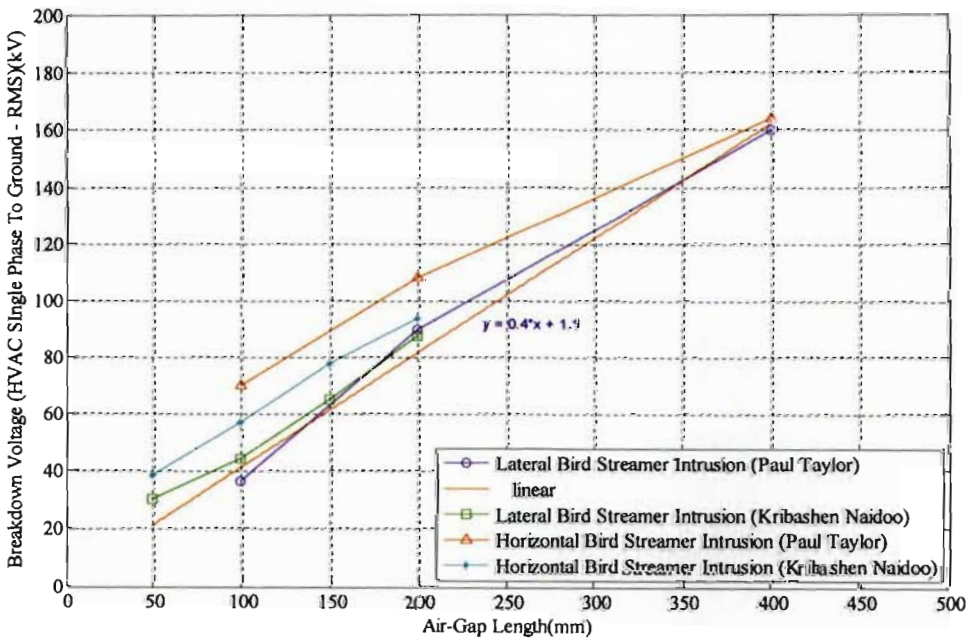

Figure 4.8 V-String experiment, lateral and horizontal air-gap breakdown, HVAC breakdown as a function of air-gap spacing

Analysis of Figure 4.8 indicates a variation in breakdown voltage for air-gap lengths in the range 100 mm to 200 mm. This variance is attributed to errors in experimental procedure between the present experiments and those of Taylor. At higher air-gap lengths (greater than 200 mm) the curves tend towards a similar gradient (shown by the linear curve in Figure 4.8).

4.2 FEM results and discussion

4.2.1 Variation in air-gap length

The results obtained for the relationship between the electric field intensity and the air-gap length is shown in Figure 4.9.

The direction of the contour chosen to calculate the electric field intensity was from the centre of the rod tip to the centre of the plane. This simulation was based on the results of Figure 4.1(a), and was done in order to explain the *principle* of either increasing or decreasing the air-gap spacing in the air-gap breakdown process, thus highlighting the streamer propagation criterion.

In Figure 4.1(a) for an air-gap length of 275 mm, the breakdown voltage was -150 kV. This simulation showed that if the air-gap length is increased, the streamer propagation criterion is not met (i.e. decrease in electric field intensity at the plane), and if the air-gap length is decreased, the streamer propagation criterion is met (i.e. increase in electric field intensity at the plane). Figure 4.9 show the relationship between the electric field intensity and the air-gap length.

The electrode configuration geometry for the experimental work, and for the QuickField™ model differ due to the two dimensional modelling capabilities of QuickField™, therefore the electric fields contained in Figure 4.9 cannot be directly applied to the experimental results.

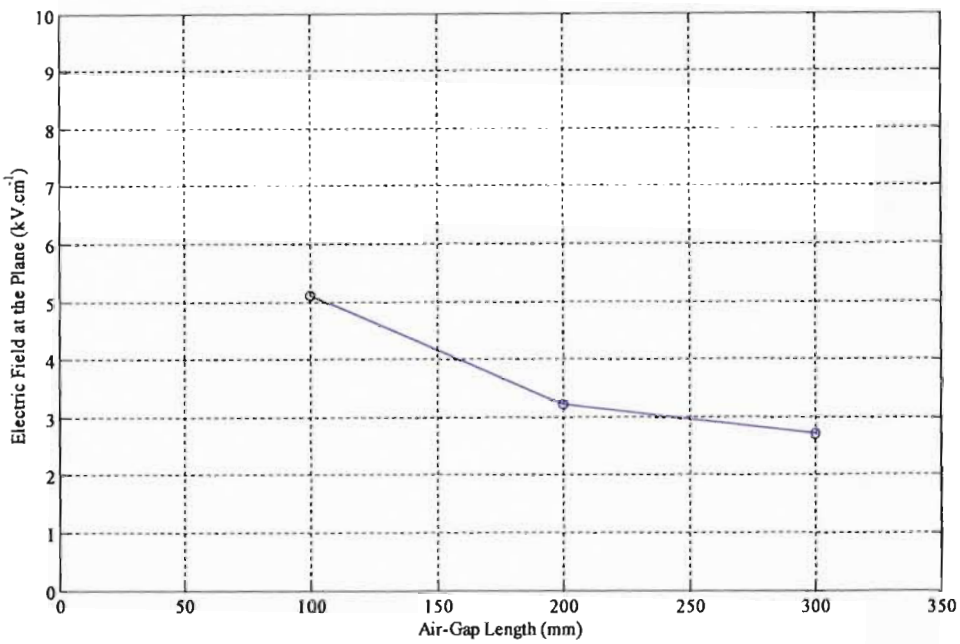

Figure 4.9 Resultant electric field intensity at the plane as the air-gap length between the electrodes increases

Figure 4.9 show that as the air-gap length between the electrodes increases (from 100 mm to 300 mm), the electric field intensity at the plane decreases. Applying this result to the case at hand, it would firstly mean that as the bird streamer descends towards the live conductor fitting, it will cause severe electric field enhancement, thus allowing for electric streamer propagation in the air-gap (this was discussed as the streamer propagation criteria in section 2.3.5). Thus, by moving the bird streamer further away from the centre of the live conductor fitting (i.e. the purpose of the protected zone), electric streamer inception will be minimised, thus minimising the bird streamer fault.

4.2.2 Variation in rod-plane electrode geometry

In this simulation, the length of the plane in the rod-plane configuration was decreased from a length of 480 mm to 10 mm. The length of the air-gap remained fixed at 50 mm in all cases. An arbitrary applied voltage of -44 kV was chosen.

Figures 4.10(a) to 4.10(e) show the relationship between the electric field intensity and the air-gap length as the length of the plane decreases. The direction of the contour chosen to calculate the electric field intensity was from the centre of the rod tip to the centre of the plane.

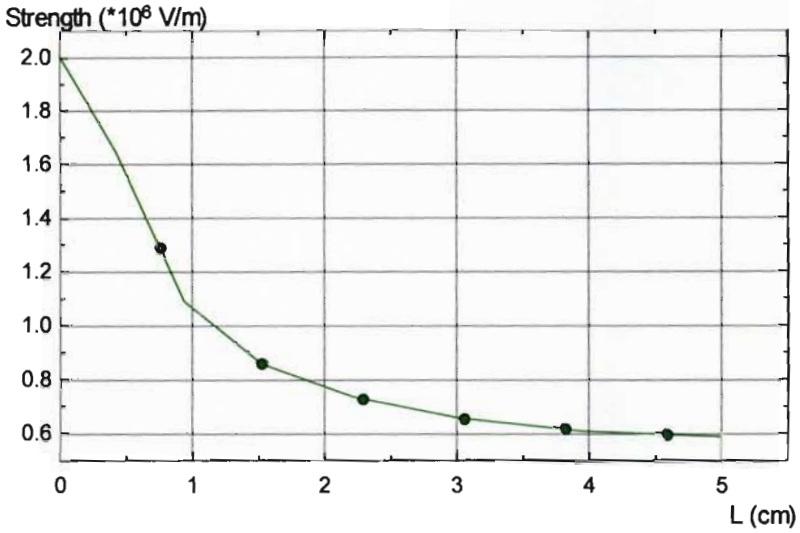

(a) 480 mm diameter plane

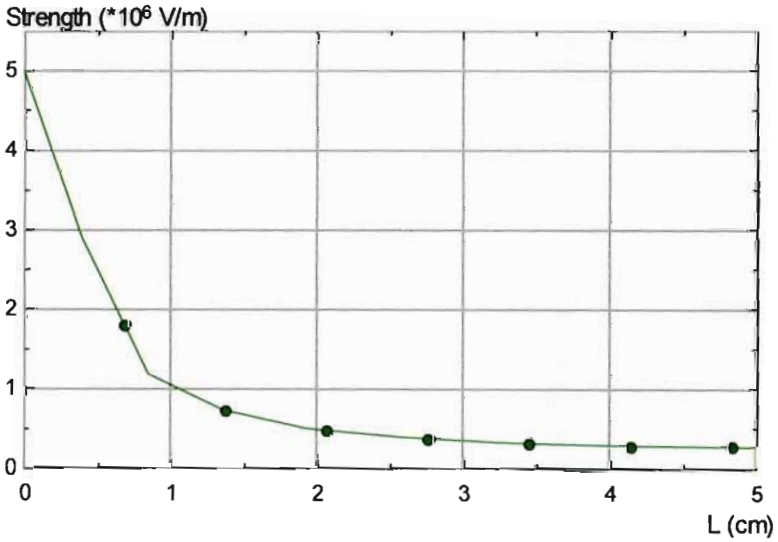

(b) 240 mm diameter plane

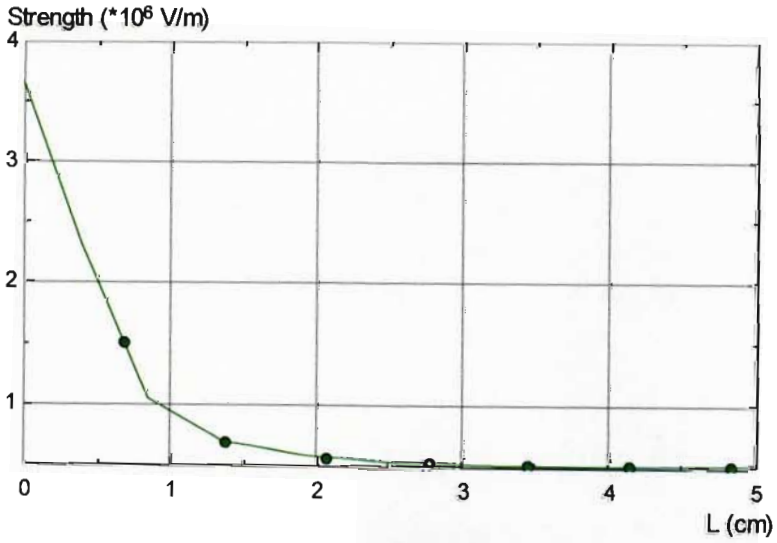

(c) 60 mm diameter plane

Figure 4.10 Resultant electric field as the geometry of the rod-plane configuration varies

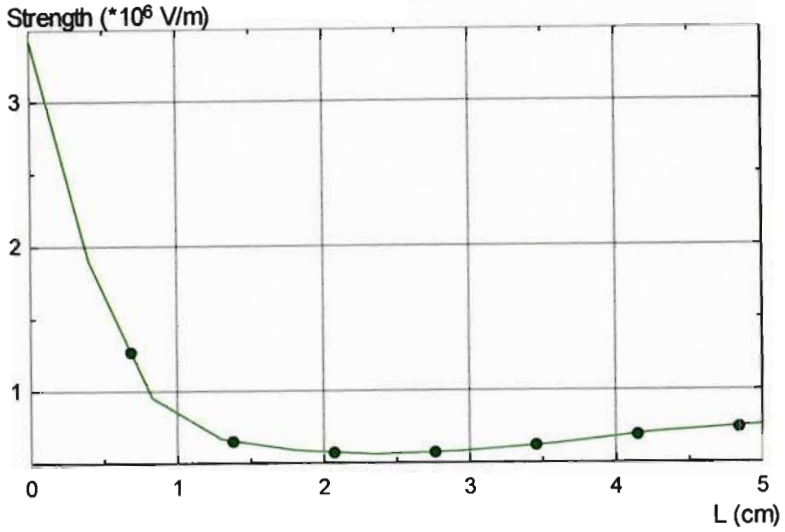

(d) 30 mm diameter plane

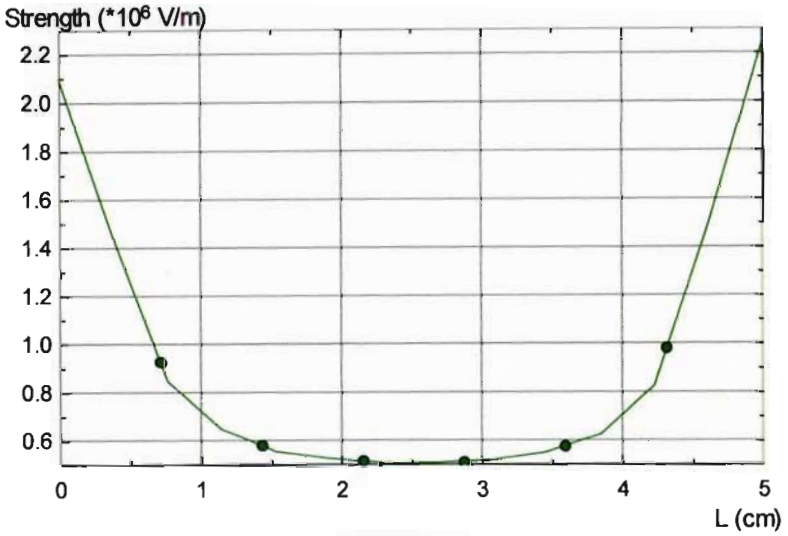

(e) 10 mm diameter plane

Figure 4.10 Resultant electric field as the geometry of the rod-plane configuration varies

The aim of these simulations was to highlight the difference in the electric field intensity curves in the air-gap between the bird streamer and the live conductor fitting as the length of the plane decreases. Figures 4.10(a) to 4.10(e) show that as the diameter of the plane decreases, a significant change in the electric field distribution along the air-gap occurs. It must be noted that the space charge influence is not catered for here, thus the true deviation in the curves cannot be observed.

This difference in electric field intensity would therefore affect the streamer propagation criteria (discussed in section 2.3.5, thus resulting in deviations of the air-gap breakdown voltages of Figure 4.1, from those of [26, 27, and 29].

4.3 Application of experimental work to the calculation of the protected zone length

The calculation of the protected zone length on an HVDC tower top incorporated the use of the breakdown voltage versus air-gap length curves from the previous sections.

This section details the methods that were used in this dissertation to calculate the protected zone length. These results were then plotted to provide a *breakdown voltage versus protected zone length* curve for both I-String and V-String insulator configurations.

4.3.1 V-String insulator configuration (HVDC)

The protected zone of a typical V-String insulator configuration was calculated for both the lateral and horizontal planes.

The lateral protected zone and the horizontal protected zone lengths are shown in Figure 4.11.

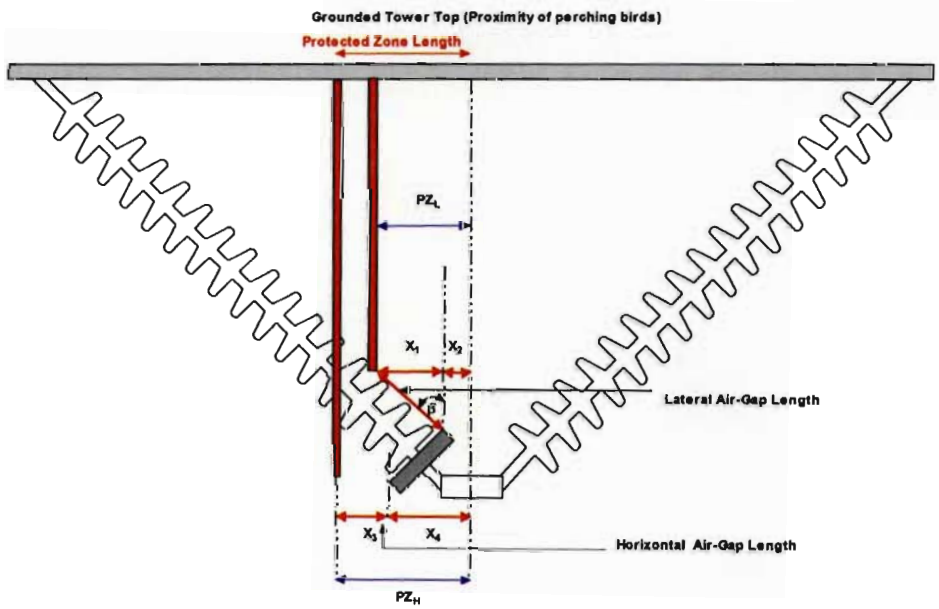

Figure 4.11 V-String insulator configuration, indication of the lateral and horizontal protected zone lengths

Figure 4.11 shows that the protected zone length in the lateral plane comprises two lengths, the sine of the angle between the vertical plane and the lateral air-gap length (β) (length X_1 in

Figure 4.11) and the distance from the centre of the live conductor fitting to the tip of the corona ring (length $X_2 = 120$ mm, in Figure 4.11).

The horizontal protected zone length plane comprises two lengths, the horizontal air-gap length (length X_3 in Figure 4.11), and the distance from the centre of the live conductor fitting to the tip of the corona ring (length $X_4 = 290$ mm, in Figure 4.11).

The length of the protected zone in the lateral and horizontal plane in a V-String insulator configuration can thus be calculated from Equations (4.1) and (4.2) respectively.

$$Lateral\ \text{Pr}\ otected\ Zone\ Length = (lateral\ airgap\ length)(\sin(\beta)) + X_2 = (X_1 + X_2) = PZ_L\ mm \qquad (4.1)$$

$$Horizontal\ \text{Pr}\ otected\ Zone\ Length = (horizontal\ airgap\ length) + X_4 = (X_3 + X_4) = PZ_H\ mm \qquad (4.2)$$

The horizontal protected zone has a greater length than the lateral protected zone, for a given air-gap length (i.e. $PZ_L < PZ_H$, for a given air-gap length).

Thus, the worst case protected zone length (i.e. greater length) is the horizontal length (shown in Figure 4.11).

The lateral and horizontal protected zone lengths were calculated for the respective air-gap lengths in order to plot the relationship between the breakdown voltage and the protected zone length (shown in Figure 4.12). Figure 4.12 (a) contains the results under negative polarity, while Figure 4.12 (b) contains the results under positive polarity.

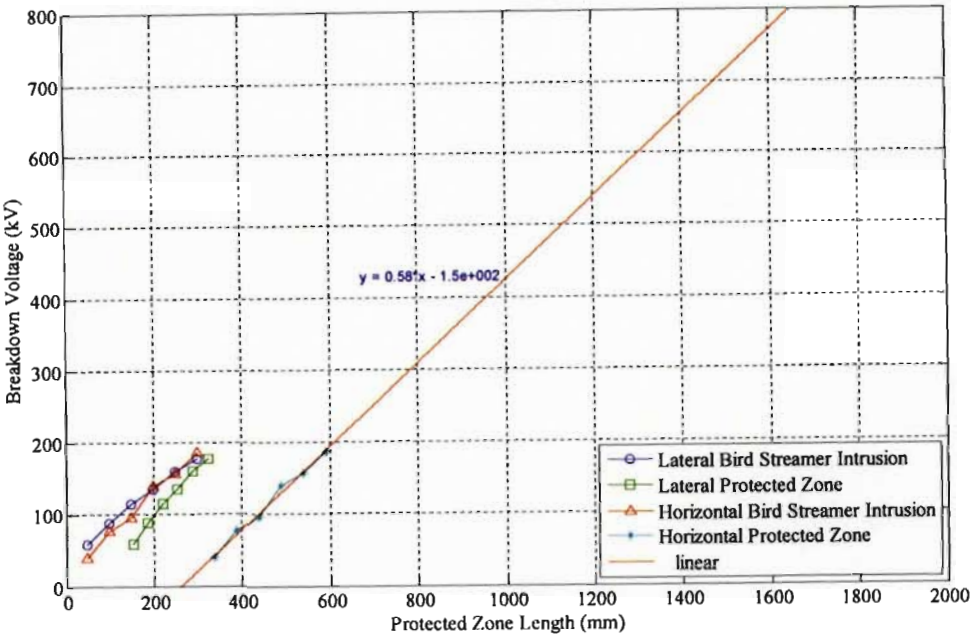

(a) Negative HVDC

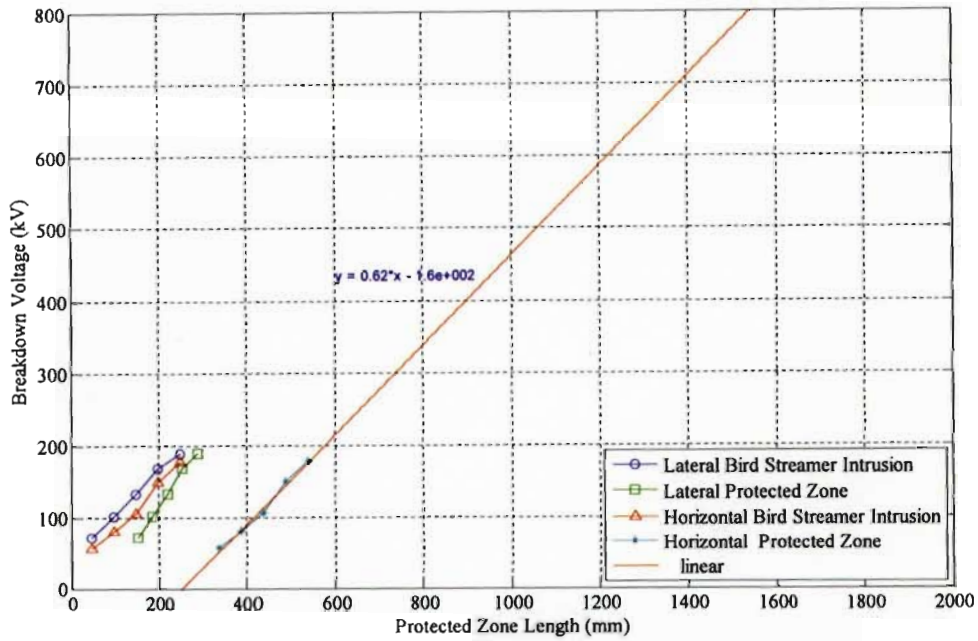

(b) Positive HVDC

Figure 4.12 V-String insulator configuration, HVDC breakdown as a function of protected zone length

Figure 4.12 shows that for a specific breakdown voltage, the horizontal protected zone length is greater than the lateral protected zone length. Thus, when choosing to protect a tower top, one would look at the lengths in the horizontal plane.

The original points in Figures 4.12 (a) and 4.12 (b) were extrapolated to provide protected zone lengths at higher breakdown voltage levels. This assumption seemed reasonable since the

relationship between the breakdown voltage and the air-gap length for both rod-plane and rod-rod electrode configurations are straight lines up to 1200 kV (HVDC) [26-30], and 500 kV (HVAC) [27].

A key point relating to Figure 4.12 is that it shows the relationship between the *breakdown voltage* and the protected zone length, and *not* the relationship between the *system voltage* and the protected zone length. Thus, when a protected zone length for a specific system voltage is needed, it cannot be directly taken from Figure 4.12. A safety factor has to therefore be used. This safety factor has to accommodate for the above mentioned technicality, the trajectory of the bird streamer and the surrounding environmental conditions. The environmental conditions can be the effect of wind on the trajectory of the bird streamer.

A safety factor of 1.4 seems reasonable to accommodate for the above factors (a safety factor of 1.1 to convert from breakdown voltage to system voltage and 1.3 for environmental conditions, $1.1 \times 1.3 \approx 1.4$).

The following example, shows the procedure used in calculating the protected zone for a system voltage of 500 kV (the value of system voltage = 500 kV is an arbitrary value). The example is based on Figure 4.12(a), since the worst case protected zone length is found under the negative polarity.

For a system voltage of 500 kV,

(i) Locate 500 kV on the y-axis of Figure 4.12(a).

(ii) Move in a horizontal direction until the horizontal protected zone curve is reached.

(iii) Note the relevant protected zone length from the abscissa; in this case it is $\approx$ 1130 mm. A more accurate method would be to use the equation of the curve provided in Figure 4.13(a), which is:

$$y = 0.58x - 150 \qquad (4.3)$$

The x co-ordinate, which is the protected zone length, can be found from a manipulation of Equation (4.3), resulting in the following equation:

$$x = \frac{y + 150}{0.58} \qquad (4.4)$$

Inputting a value of 500 for *y* yields a protected zone length of 1120 mm.

(iv) Multiplying this length by a safety factor of 1.4, yields a protected zone length of 1568 mm.

(It should be noted that this length refers to one half of the full protected zone length on a V-String tower, i.e. it should be multiplied by a factor of 2 in order to cater for the entire tower top. This can be ignored in case of the I-String insulator configuration.)

4.3.2 I-String insulator configuration (HVDC)

The protected zone of an I-String insulator configuration can be calculated for the horizontal plane only.

The horizontal protected zone length is indicated in Figure 4.13.

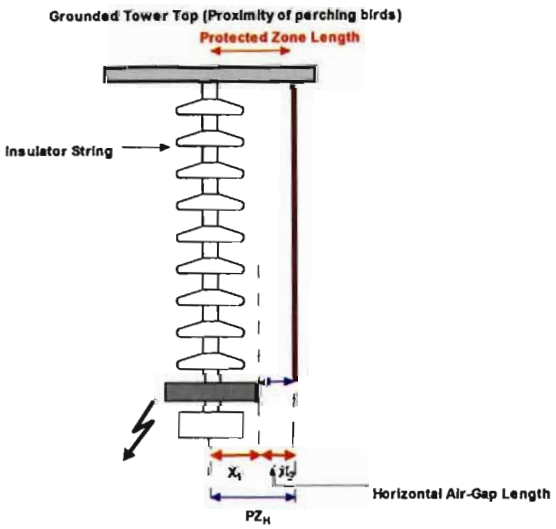

Figure 4.13 I-String insulator configuration, indication of the horizontal protected zone length

The horizontal protected zone length is the sum of the horizontal air-gap length and the distance from the centre of the insulator string to the streamer tip (length X_1 in Figure 4.13).

The length of the protected zone in the case of the I-String insulator configuration can thus be calculated from Equation (4.5).

$$Horizontal\ \text{Pr}\ otected\ Zone\ Length = (horizontal\ airgap\ length) + X_2 = X_1 + X_2 = PZ_H\ mm \qquad (4.5)$$

Using the above equation, the protected zone lengths for the respective air-gap lengths were calculated in order to plot the relationship between the breakdown voltage and the protected

zone length (shown in Figure 4.14). Figure 4.14 (a) contains the results under negative polarity, while Figure 4.14 (b) contains the results under positive polarity.

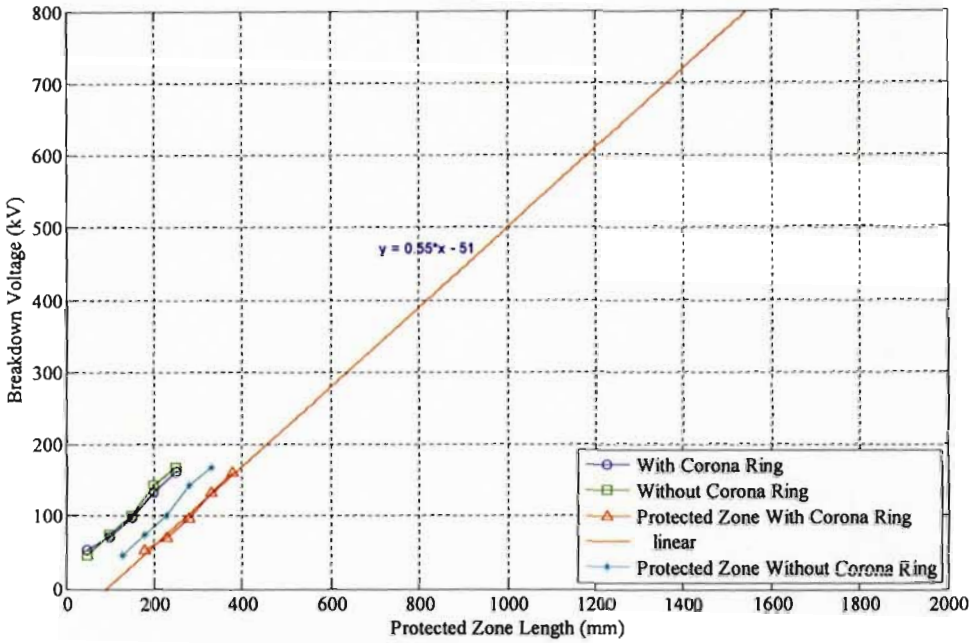

(a) *Negative HVDC*

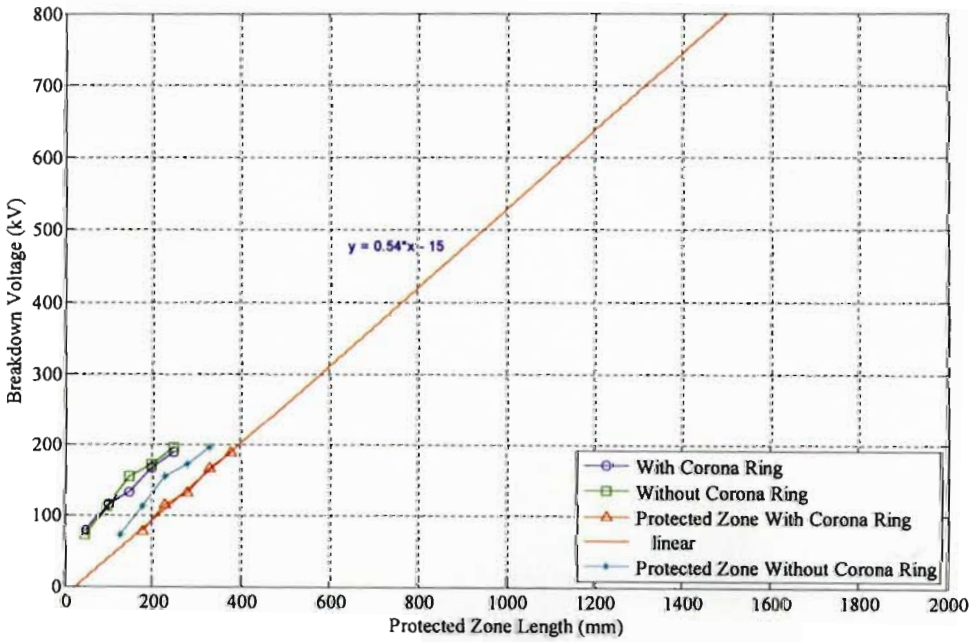

(b) Positive HVDC

Figure 4.14 ***I-String insulator configuration, HVDC breakdown as a function of protected zone length***

Figure 4.14 shows the relationship between the breakdown voltage and the protected zone length, and not the relationship between the system voltage and the protected zone length. The statements relating to system voltage and the trajectory of the bird streamer of section 4.2.1 remain the same for this case, thus a safety factor of 1.4 should be used.

4.3.3 Comparison of protected zone lengths for brass rod and soaked string

This section details the differences in protected zone lengths between a soaked string and a brass rod. For the soaked string, the results of Figure 4.1 were used in this comparison. The negative polarity protected zone lengths from previous sections were used (The V-String results with a corona ring were used.), since they produced the longer protected zone lengths. This comparison was made in order to assess the differences in using a brass rod and a soaked string as the artificial bird streamer.

Figure 4.15 shows the relationship between the breakdown voltage and the protected zone length for the horizontal air-gap breakdown.

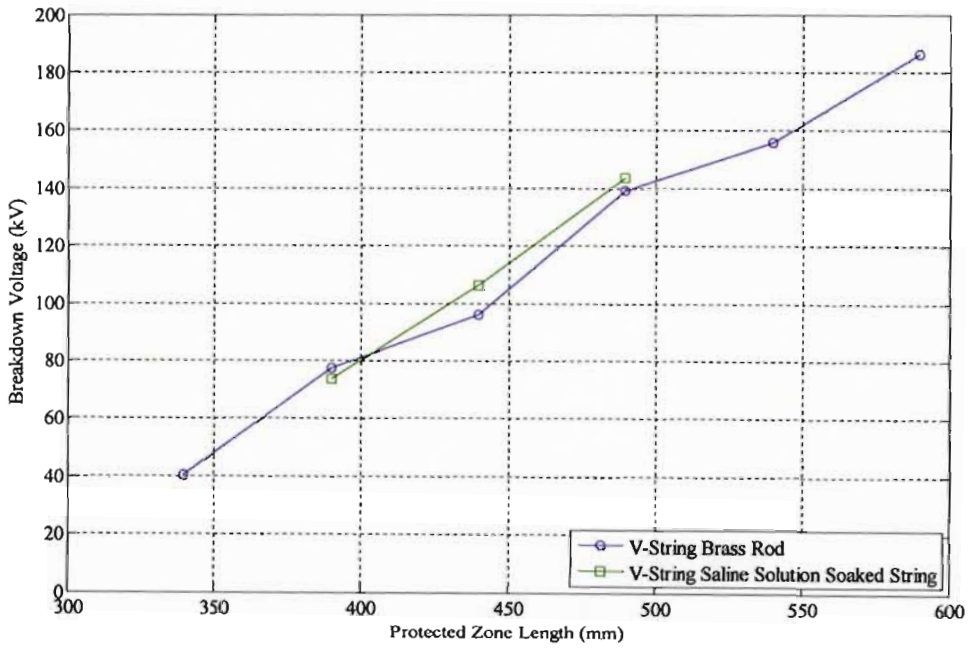

Figure 4.15 Comparison of protected zone lengths for a brass rod and soaked string

Analysis of Figure 4.15 indicates a small difference in protected zone lengths for both the artificial bird streamers. These results confirm that that a brass rod is an acceptable artificial streamer, with small deviations from that of a soaked string.

4.3.4 V-String insulator configuration (HVAC)

Equations (4.1) and (4.2) of section 4.2.1, are equally applicable in the HVAC case.

Figure 4.16 shows the relationship between the breakdown voltage and the protected zone length for the horizontal air-gap breakdown.

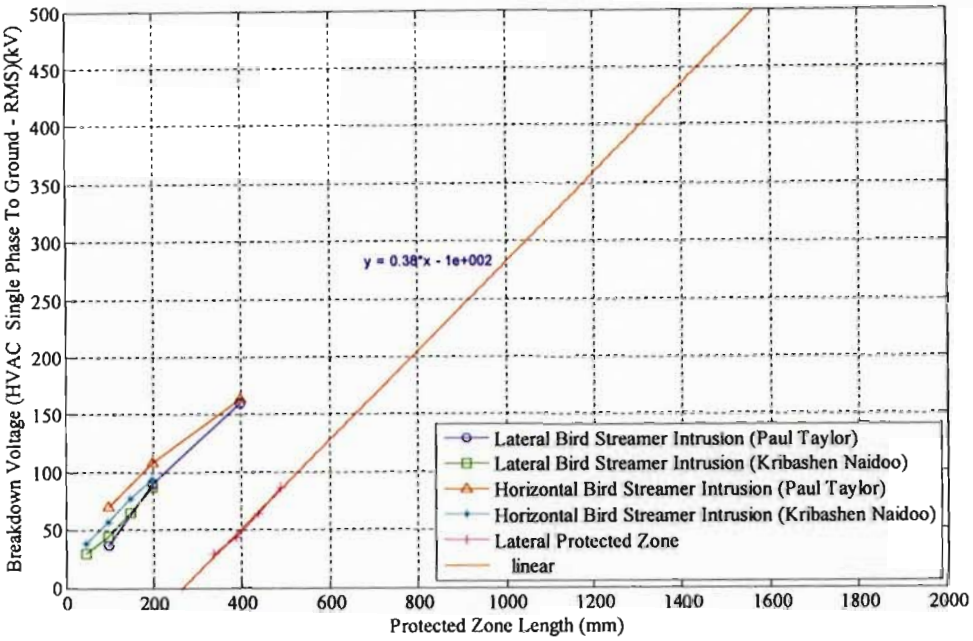

Figure 4.16 V-String insulator configuration, *HVAC* breakdown as a function of protected zone length

The statements relating to system voltage and the trajectory of the bird streamer of section 4.2.1 remain the same for the HVAC case. Thus a safety factor of 1.4 should be used in this case.

A comparison of the protected zone lengths found by Taylor [6], Hoch et al [11] and the present author is shown in Table 4.1.

Table 4.1 Comparison of current protected zone lengths with previous researcher's findings

System Voltage (kV)	*Equivalent Single Phase Voltage (kV)*	*Insulator Configuration*	*Protected Zone Length• (mm) Taylor [6]*	*Protected Zone Length (mm) Hoch [11]*	*Protected Zone Length▪ (mm) Naidoo [Present Work]*
275	160	V-String (With Corona Ring)	900	700	960 (685) ▲
220	127	V-String (With Corona Ring)	…	500	840 (600) ▲
132	76	V-String (With Corona Ring)	…	500	660 (470) ▲
132	76	V-String (No Corona Ring	…	500	…

Note: ■ These protected zone lengths include a safety factor of 1.4, the calculations of which are shown in Appendix C.

▲These protected zones lengths do not include a safety factor.

• This protected zone lengths includes a safety factor of 2

A key point to note in Table 4.1 is that the protected zone lengths shown for Taylor include a safety factor of 2, while the protected zone lengths for Hoch are the pure experimental results with no safety factor added. The present author's results with the exclusion of a safety factor are similar to that of Hoch *et al*, proving that the method used for calculating the protected zone is in line with previous experimental work.

4.3.5 Floating bird streamer

Figure 4.6 shows that as the bird streamer descends from the grounded tower top, the application of the high voltage, interchanges from the plane to the rod, thus providing greater breakdown voltages under negative polarity.

Figure 4.6 also shows that the breakdown strength is much higher towards the centre of the bird streamer path (i.e. when $D_1 = D_2$), between the tower top and the live conductor fitting.

The above mentioned alterations in the relationship between the breakdown voltage and the air-gap length under negative polarity will thus lead to:

(i) Shorter overall protected zone lengths under both HVDC and HVAC conditions.

This experiment delved into the study of the floating bird streamer. Further work is necessitated in this area, to firstly prove that the floating bird streamer is existent, and if its existence is verified, more experiments need to be performed. These experiments should look at the effect of varying the length of the streamer in a fixed air-gap length, which was not performed in this dissertation.

4.4 Discussion

4.4.1 Experimental results

This Chapter has provided a method for calculating the protected zone length for both I-String and V-String insulator configurations. The formulas and methods are adaptable for various suspension angles and either HVAC or HVDC conditions

The critical factors that determine the protected zone length have been brought to the foreground, these being the breakdown voltage for a specific air-gap length, and the lengths X_2, X_4 and X, mentioned earlier.

A rough estimate for the equation of the protected zone curve (Figure 4.12 (a)) in the DC can be found from the protected zone curve (Figure 4.16) in the AC case. This relation is:

$$y = \frac{HVAC\ gradient}{0.62} x - 150 \qquad (4.6)$$

(The HVAC gradient can be taken from Figure 4.13)

From this relationship, it can be noted that the bird streamer under HVDC conditions has a higher voltage withstand than under HVAC conditions, but this is only valid up to a voltage level of 500 kV, thereafter, the HVAC curve becomes non-linear [26].

The length of the bird streamer is a key factor in determining whether a bird streamer will cause a line fault. A simple calculation was performed in order to verify whether a fault caused by a bird streamer could be possible on the Apollo-Songo line.

The total air-gap length between the grounded region and the nearest live hardware is taken to be 4.16 m, while the operating voltage of the line is ≈ 500 kV [5]. The breakdown strength is chosen to be 5.5 $kV.cm^{-1}$ (from Figure 4.15). The bird streamer length is assumed to be 3.3 m [35]. The remaining air-gap length is thus equal to 4.16 m – 3.3 m = 0.86 m. The voltage required to bridge the remaining air-gap (0.86 m) can be found by multiplying 5.5 $kV.cm^{-1}$ by the remaining air-gap length, which yields a voltage of 473 kV. This voltage is within the system voltage limits, thus a bird streamer caused fault is possible on the Apollo- Songo line.

As the voltage of a line increases so too does the air-gap length. This would mean that the likelihood of a bird caused streamer fault is reduced, due to the maximum streamer length given

above. To prove this, a similar calculation was performed, pertaining to an 800 kV line. The relevant line data was obtained from Britten [36], (the total air-gap length between the grounded region and the nearest live hardware is taken to be 8 m). Using a similar calculation method as above, results in a remaining air-gap length equal to 8 m – 3.3 m = 4.7 m. This would therefore result in a voltage of 2585 kV. This voltage is significantly above the system voltage of 800 kV. This proves that as the voltage level increases, the likelihood of a bird streamer caused fault is reduced.

This chapter has also looked at the streamer conductivity on the breakdown process. A higher conductivity leads to lower breakdown voltage, and vice versa.

4.4.2 FEM results

The results of the field analysis show how the maximum electric field intensity increases with a decrease in air-gap length. In the case of the decrease in air-gap length, the highest electric field intensity occurs when the rod was closest to the plane (i.e. the shortest air-gap length). In the case of the variation in the plane length, the electric field intensity changes as the length of the plane changes.

4.5 Conclusion

This chapter has shown the relationship between the breakdown voltage and the length of the air-gap between the bird streamer tip and the live conductor fitting. From these relationships, a curve describing the protected zone length for various breakdown voltages has been developed.

The FEM results indicate how the probability of air-gap breakdown is decreased as the bird streamer is moved away from the live conductor fitting.

5 CONCLUSIONS AND FURTHER WORK

In this dissertation a set of formulas has been developed to calculate the protected zone length on an HVDC tower top. These formulas are based on data gained from the relationship between the breakdown voltage and the length of the air-gap between a bird streamer tip and the live conductor fitting.

A curve has been derived, whereby the protected zone length can be found for a particular system voltage. This will assist tower design engineers by providing an aid, which can be used in the design to minimise the occurrence of bird streamer induced faults.

The formulas are applicable to either V-String or I-String insulator configurations at sea-level conditions.

In particular, the following conclusions can be drawn from this dissertation:

(i) The bird streamer fault under the HVDC conditions requires a shorter protected zone length than under HVAC conditions (valid for a value of up to 500 kV AC rms)

(ii) The variation in conductivity in the range 10 μS to 10 000 μS, is small because the breakdown voltages are very similar.

(iii) The time-of-day analysis is a useful tool in identifying faults caused by birds, but needs to be adapted to local conditions.

The research has provided knowledge of bird streamer faults in the HVDC case. The following recommendations for possible further work in this research area include:

(i) Experimental work needs to be done on this fault type at higher DC voltages. This will provide further evidence as to what voltage levels this fault will pose a problem. In doing so, the length of bird streamer required to cause breakdown at higher system voltages will be gained. These experiments should look at the liquid streamer, and will thus take into effect the dynamic bird streamer in the air-gap breakdown process.

(ii) Innovation in bird guard design is needed, in order to provide efficient use of the protected zone lengths curves provided in this dissertation.

(iii) The need for an investigative report, detailing the conductivity and the length of a bird streamer for different species of birds.

(iv) Experimental work, detailing the affect of humidity on the air-gap breakdown process.

Appendix A

(i) Rod-Plane Arrangement

Table A.1 10 mm brass rod-live conductor fitting, negative & positive DC

Air Gap Length (mm)	*Negative DC*		*Positive DC*	
	Voltage ■ (kV)	*Corrected Voltage (kV)*	*Voltage ▲ (kV)*	*Corrected Voltage (kV)*
50	44.2	43.2	65.4	62.8
100	62.2	65.6	92.9	89.3
150	93.4	91.2	115.1	110.6
200	113.2	114.5	144.9	139.2
250	143.3	140.0	168.6	162.0
300	163.4	159.6	195.3	187.7

Note: ■ Temperature: 18.8 °C, Pressure: 985.2 mb, Humidity: 51.8 %

▲ Temperature: 22.0 °C, Pressure: 980.0 mb, Humidity: 60.0 %

Table A.2 Short air-gap, negative DC

Air Gap Length (mm)	*Case 2 ■ (kV)*	*Corrected Voltage (kV)*	*Case 4 ■ (kV)*	*Corrected Voltage (kV)*
10	16.0	15.8	21.0	20.8
20	31.0	30.6	39.7	39.2
30	40.7	40.2	53.7	53.1
40	48.7	48.1	70.0	69.2
50	59.0	58.3	87.7	86.7
60	66.7	65.9	104.7	103.5

Note: ■ Temperature: 21.2 °C, Pressure: 1005.4 mb, Humidity: 45.0 %

Table A.3 Short air-gap, positive DC

Air Gap Length (mm)	*Case 1 ■ (kV)*	*Corrected Voltage (kV)*	*Case 3 ■ (kV)*	*Corrected Voltage (kV)*
10	21.3	21.1	15.7	15.5
20	39.0	38.5	31.3	30.9
30	53.7	53.1	40.3	39.8
40	67.7	66.9	48.6	48.0
50	83.6	79.7	56.3	53.7
60	104.0	102.8	63.7	60.0

Note: ■ Temperature: 21.2 °C, Pressure: 1005.4 mb, Humidity: 45.0 %

Table A.4 Rod-Rod air-gap, positive and negative DC

Air Gap Length (mm)	*Negative DC* ■ (kV)	*Corrected Voltage* (kV)	*Positive DC* ■ (kV)	*Corrected Voltage* (kV)
50	46	45.4	44.7	44.1
100	70	69.1	66.3	65.4
150	96	94.7	88.6	87.4
200	116	114.5	113.5	112.0
250	...	...	128.2	126.5

Note: ■ Temperature: 20.2 ^{0}C, Pressure: 1000.4 mb, Humidity: 48.0 %

Table A.5 Rod-Plane air-gap, positive and negative DC

Air Gap Length (mm)	*Negative DC* ■ (kV)	*Corrected Voltage* (kV)	*Positive DC* ■ (kV)	*Corrected Voltage* (kV)
25	...	...	58	57.2
50	49	48.4	108	106.2
100	65	64.1	176	173.7
150	102	100.7	...	...

Note: ■ Temperature: 20.2 ^{0}C, Pressure: 1000.4 mb, Humidity: 48.0 %

Table A.6 Floating bird streamer, negative DC

Air Gap Length (mm)	*Negative DC* ▲ (kV)	*Corrected Voltage* (kV)
0	193.6	193.2
50	209.3	208.9
100	216.3	215.9
150	219.3	218.9
175	217.9	217.5
200	216.5	216.1
250	216.0	215.6
300	213.8	213.4
350	205.6	205.2

Note: ▲ Temperature: 20.9 ^{0}C, Pressure: 1014.1 mb, Humidity: 56.7 %

Table A.7 Soaked string-live conductor fitting, negative DC

Air Gap Length (mm)	*10 μS.cm^{-1} Solution* ▪ *(kV)*	*Corrected Voltage (kV)*	*10 000 μS.cm^{-1} Solution* ▪ *(kV)*	*Corrected Voltage (kV)*
100	80.2	79.2	74.1	73.2
150	129.4	127.8	107.3	105.9
200	152.3	150.4	145.0	143.2

Note: ▪ Temperature: 20.7 °C, Pressure: 1002.5 mb, Humidity: 52.4 %

Table A.8 Soaked string-live conductor fitting, positive DC

Air Gap Length (mm)	*10 μS.cm^{-1} Solution* ▪ *(kV)*	*Corrected Voltage (kV)*	*10 000 μS.cm^{-1} Solution* ▪ *(kV)*	*Corrected Voltage (kV)*
100	107.9	106.1	99.1	97.5
150	141.2	138.9	133.4	131.2
200	167.3	164.5	166.2	163.5

Note: ▪ Temperature: 21.2 °C, Pressure: 1000.5 mb, Humidity: 51.4 %

(ii) V-String Insulator Configuration

Table A.9 V-String, brass rod, lateral intrusion, negative and positive DC

Air Gap Length (mm)	*Negative DC* ▪ *(kV)*	*Corrected Voltage (kV)*	*Positive DC* ▲ *(kV)*	*Corrected Voltage (kV)*
50	58.2	57.7	73.3	72.8
100	88.6	87.9	102.1	101.5
150	115.6	114.7	134.6	133.8
200	136.2	135.2	169.2	168.2
250	160.9	159.7	190.2	189.1
300	177.8	176.5	…	…

Note: ▪ Temperature: 19.2 °C, Pressure: 1002.6 mb, Humidity: 55.9 %

▲ Temperature: 18.4 °C, Pressure: 1001.5 mb, Humidity: 63.1 %

Table A.10 V-String, brass rod, horizontal intrusion, negative and positive DC

Air Gap Length (mm)	*Negative DC* ■ *(kV)*	*Corrected Voltage (kV)*	*Positive DC* ▲ *(kV)*	*Corrected Voltage (kV)*
50	40.6	40.2	58.5	57.5
100	78.2	77.4	82.8	81.4
150	97.1	96.1	108.5	106.7
200	140.4	138.9	152.3	149.8
250	157.6	156.0	181.3	178.3
300	188.3	186.3	...	...

Note: ■ Temperature: 20.2 °C, Pressure: 1003.1mb, Humidity: 52.4 %

▲ Temperature: 21.4 °C, Pressure: 1001.2 mb, Humidity: 64.1%

Table A.11 V-String, brass rod, lateral and horizontal intrusion, HVAC

Air Gap Length (mm)	*Lateral Breakdown Voltage* ■ *(kV)*	*Corrected Voltage (kV)*	*Horizontal Breakdown Voltage* ▲ *(kV)*	*Corrected Voltage (kV)*
50	30.72	30.04	39.22	38.36
100	45.30	44.30	58.46	57.17
150	66.62	65.15	79.24	77.49
200	89.22	87.25	95.80	93.69

Note: ▲ Temperature: 22.2 °C, Pressure: 998.1mb, Humidity: 50.4 %

(iii) I-String Insulator Configuration

Table A.12 I-String, brass rod, horizontal intrusion, negative DC

Air Gap Length (mm)	*Without Corona Ring*		*With Corona Ring*	
	DC Voltage ■ *(kV)*	*Corrected Voltage (kV)*	*DC Voltage* ▲ *(kV)*	*Corrected Voltage (kV)*
50	46.1	46.1	54.1	54.1
100	74.2	74.1	70.2	70.1
150	100.1	100.0	98.1	98.0
200	141.9	141.8	132.9	132.8
250	167.5	167.4	160.5	160.4

Note: ■ Temperature: 18.2 °C, Pressure: 1005.9 mb, Humidity: 36.4%

▲ Temperature: 20.9 °C, Pressure: 1014.1 mb, Humidity: 56.7 %

Table A.13 I-String, brass rod, horizontal intrusion, positive DC

Air Gap Length (mm)	*Without Corona Ring*		*With Corona Ring*	
	Breakdown Voltage ■ *(kV)*	*Corrected Voltage (kV)*	*Breakdown Voltage* ▲ *(kV)*	*Corrected Voltage (kV)*
50	72.5	72.0	79.2	78.6
100	113.5	112.7	117.2	116.3
150	155.3	154.2	134.2	133.2
200	173.3	172.0	168.3	167.1
250	196.5	195.1	190.3	189.0

Note: ■ Temperature: 20.1 °C , Pressure: 1005.9 mb, Humidity: 50.9 %

▲ Temperature: 19.8 °C, Pressure: 1000.2 mb, Humidity: 42.4 %

(iv) Protected zone lengths

Table A.14 V-String, lateral and horizontal protected zone lengths, negative DC

Lateral Protected Zone Length (mm)	*Breakdown Voltage* ■ *(kV)*	*Corrected Voltage (kV)*	*Horizontal Protected Zone Length (mm)*	*Breakdown Voltage* ▲ *(kV)*	*Corrected Voltage (kV)*
154	67.2	66.7	340	40.6	40.2
188	88.6	87.9	390	78.2	77.4
222	115.6	114.7	440	97.1	96.1
256	136.2	135.2	490	140.4	138.9
290	160.9	159.7	540	157.6	156.0
325	177.8	176.5	590	188.3	186.3

Note: ■ Temperature: 19.2 °C, Pressure: 1002.6 mb, Humidity: 55.9 %

■ Temperature: 20.2 °C, Pressure: 1003.1mb, Humidity: 52.4%

Table A.15 V-String, lateral and horizontal protected zone lengths, positive DC

Lateral Protected Zone Length (mm)	*Breakdown Voltage* ■ *(kV)*	*Corrected Voltage (kV)*	*Horizontal Protected Zone Length (mm)*	*Breakdown Voltage* ▲ *(kV)*	*Corrected Voltage (kV)*
154	80.3	79.8	340	58.5	57.5
188	102.1	101.5	390	82.8	81.4
222	134.6	133.8	440	108.5	106.7
256	169.2	168.2	490	152.3	149.8
290	190.2	189.1	540	181.3	178.3

Note: ■ Temperature: 18.4 °C, Pressure: 1001.5 mb, Humidity: 63.1 %

▲ Temperature: 21.4 °C, Pressure: 1001.2 mb, Humidity: 64.1%

Table A.16 I-String, horizontal protected zone lengths, negative DC

Protected Zone Length (mm) (With Corona Ring)	*Breakdown Voltage* ■ *(kV)*	*Corrected Voltage (kV)*	*Protected Zone Length (mm) (Without Corona Ring)*	*Breakdown Voltage* ▲ *(kV)*	*Corrected Voltage (kV)*
180	54.1	54.1	130	46.1	46.1
230	70.2	70.1	180	74.2	74.1
280	98.1	98.0	230	100.1	100.0
330	132.9	132.8	280	141.9	141.8
380	160.5	160.4	330	167.5	167.4

Note: ■ Temperature: 20.9 ^{0}C, Pressure: 1014.1 mb, Humidity: 56.7 %
▲ Temperature: 18.2 ^{0}C, Pressure: 1005.9 mb, Humidity: 36.4%

Table A.17 I-String, horizontal protected zone lengths, positive DC

Protected Zone Length (mm) (With Corona Ring)	*Breakdown Voltage* ■ *(kV)*	*Corrected Voltage (kV)*	*Protected Zone Length (mm) (Without Corona Ring)*	*Breakdown Voltage* ▲ *(kV)*	*Corrected Voltage (kV)*
180	79.2	78.6	130	72.5	72.0
230	117.2	116.3	180	113.5	112.7
280	134.2	133.2	230	155.3	154.2
330	168.3	167.1	280	173.3	172.0
380	190.3	189.0	330	196.5	195.1

Note: ■ Temperature: 19.8 ^{0}C, Pressure: 1000.2 mb, Humidity: 42.4 %
▲ Temperature: 20.1 ^{0}C , Pressure: 1005.9 mb, Humidity: 50.9 %

Table A.18 V-String, lateral and horizontal protected zone lengths, HVAC

Lateral Protected Zone Length (mm)	*Breakdown Voltage (kV)*	*Corrected Voltage (kV)*	*Horizontal Protected Zone Length (mm)*	*Breakdown Voltage (kV)*	*Corrected Voltage (kV)*
154	30.72	30.04	340	39.22	38.36
188	45.30	44.30	390	58.46	57.17
222	66.62	65.15	440	79.24	77.49
256	89.22	87.25	490	95.80	93.69

Note: ▲ Temperature: 22.2 ^{0}C, Pressure: 998.1mb, Humidity: 50.4 %

Appendix B

MACLEAN POWER SYSTEMS
Reliable Power Products
11411 Addison, Franklin Park, IL 60131 USA (847) 455-0014

Catalog Number:		**S178058VX18**
Date:		10/31/2005
END FITTINGS / MATERIAL		
Tower End Fitting:		Socket (IEC 16)
Line End Fitting:		Ball (IEC 16)
Corona Ring (tower):		none
Corona Ring (line):		none
Number of Sheds:		25
Weight Estimate:	13.2 Lbs	6.0 kg
DIMENSIONAL VALUES		
Section Length (A):	58 In	1,473 mm
Shed Diameter (B):	5.1 In	129 mm
Shed Spacing (C):	1.94 In	49 mm
Dry Arc Distance:	48.9 In	1,241 mm
Leakage Distance:	144.1 In	3,659 mm
ELECTRICAL VALUES		
60 Hz Dry F.O.(Min. Withstand):	480 kV	(443 kV)
60 Hz Wet F.O.(Min. Withstand):	428 kV	(373 kV)
CIFO + (Min. Withstand):	821 kV	(713 kV)
CIFO - (Min. Withstand):	869 kV	(762 kV)
MECHANICAL VALUES		
Specified Mech. Load (SML):	27,000 Lbs	120.1 kN
Routine Test Load (RTL):	13,500 Lbs	60.1 kN

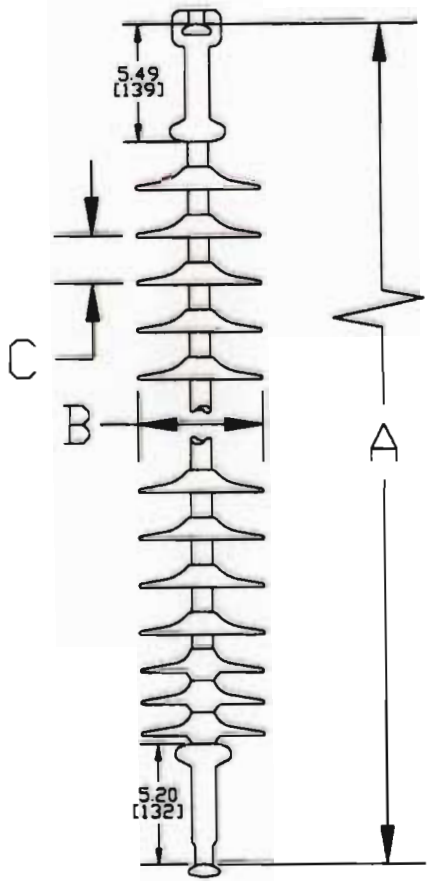

Approved	S1718058VX	0025	BAM

Silicone Rubber Sheath & Sheds
Complies with applicable ANSI and IEC standards.

Appendix C

The steps used to obtain the results in Table 4.1 are shown below:

For a system voltage of 275 kV, the equivalent single phase to earth voltage is 160 kV.

(i) Locate 160 kV on the y-axis of Figure 4.11

(ii) Move in a horizontal direction until the protected zone curve is met.

(iii) Note the relevant protected zone length from the abscissa; in this case it is 685 mm.

(iv) Multiply this length by a safety factor of 1.4, this yields a protected zone length of 960 mm.

The same procedure was followed for the 220 kV and 132 kV system voltages.

REFERENCES

[1] J. Arillaga, *High Voltage Direct Current Transmission*, Second Edition, London, Peter Peregrinus Ltd., 1983.

[2] Siemens, "High Voltage Direct Current-Proven Technology for Power Exchange", http://www.rmst.co.il/HVDC_Proven_Technology.pdf. Last accessed on the fourth of November, 2006.

[3] R. Rudervall, J.P. Charpentier, and R. Sharma, "High Voltage Direct Current Transmission Systems Technology Review Paper", Energy Week 2000, March 2000.

[4] C. van Rooyen, "The fundamentals and practices of overhead line maintenance", Crown Publishers CC, March 2004, (Chapter 11).

[5] F.F. Bologna, A.C. Britten, R.E. Kohlmeyer and H.F. Vosloo, "Investigation into the Cause of "Unknown" Line Faults on a ± 533 kV DC Line in South Africa", *Proceedings of the HVDC 2006 Congress*, University of KwaZulu-Natal, Durban, 2006, Paper 18.

[6] P. Taylor, "Case Study of Bird Streamer Caused Transient Earth Faults on a 275 kV Transmission Grid", Master's Thesis, University of Natal, 2001.

[7] R. Sundarajan, J. Burnham, R. Charlton, E.A. Cherney, G. Couret, K.T. Eldridge, M. Farzaneh, S.D. Frazier, R.S. Gorur, R. Harness, D, Shaffner, S, Siegel and J. Varner, "Preventive Measures to Reduce Bird-Related Power Outages - Part 2: Streamer and Contamination", *IEEE Transactions on Power Delivery*, Vol. 19, No. 4, pp. 1848-1853, 2004.

[8] H. West, J. Brown and A. Kinyon, "Simulation of EHV transmission line flashovers initiated by bird excretion", *Proceedings of the PES Winter Power Meeting*, 1971, Paper 71, TP 145-PWR.

[9] EPRI Report EL5735, "A joint power utility investigation of unexplained transmission line outages", 1998,

[10] J.T. Burnham, "Bird Streamer Flashovers on FP&L Transmission Lines", *IEEE Transactions on Power Delivery*, Vol. 10, No. 2, pp. 970-977, 1995.

[11] D.A. Hoch, and F. Bologna, "Laboratory Study of Bird Streamer Flashover Mechanism for different Voltages and Hardware Arrangements", Eskom, Technical Report RES/RR/02/18249, March 2003.

[12] J.M. Seifert, "Investigations of Bird Streamer Flashovers at 400 kV Overhead Transmission Line Composite Insulator Sets", *Proceeding of the Thirteenth International Symposium on High Voltage Engineering*, Rotterdam, Netherlands, 2003.

[13] X. Wang, L. Xidong, Y. Zhou, S. Wang and Z. Guan, "Composite insulator flashover caused by bird dropping and unknown reasons", *Proceeding of the Thirteenth International Symposium on High Voltage Engineering*, Rotterdam, Netherlands, 2003.

[14] IEEE Task Force, "Preventive Measures to Reduce Bird-Related Power Outages – Part 1: Electrocution and Collision", *IEEE Transactions on Power Delivery*, Vol. 19, No. 4, pp. 1843-1847.

[15] P. S. Maruvada, Corona Performance of High Voltage Transmission Lines, Research Studies Press Ltd, 2000, (Chapter Three).

[16] V. Cooray, "The Lightning Flash", IEE Power Series, 2003, (Chapter Three).

[17] E. Kuffel, W.S. Zaengl, J. Kuffel, "High Voltage Engineering Fundamentals", Pergamon Press, 2000, (Chapter Five).

[18] T. Suzuki, "Breakdown Process in rod-plane gaps with DC voltages", *IEEE Transactions*, Vol. 1A-21, pp. 26-34, 1985.

[19] N.L. Allen, and M. Boutlendj, "Study of the Electric Fields Required for Streamer Propagation in Humid Air", *IEE Proceedings*, Vol. 138, No. 1, pp. 37-43, 1991.

[20] R. Sundarajan, and R.S. Gorur, "Dynamic Arc Modelling of Pollution Flashover of Insulators under DC Voltage", *IEEE Transactions on Electrical Insulation*, Vol. 28, No. 2, pp. 209-218, 1993.

[21] T. Suzuki, "Transition from the Primary Streamer to the Arc in Positive Point-Plane Corona", *Journal of Applied Physics*, Vol. 42, No. 10, pp. 3766-3777, 1971.

[22] E. Marode, "The mechanism of spark breakdown in air at atmospheric pressure between a positive point and a plane. 1. Experimental: Nature of the streamer track", *Journal of Physics D: Applied Physics*, Vol.46, pp. 2005-2015, 1975.

[23] A. Larsson, "The effect of a Large Series Resistance on The Streamer-To-Spark Transition in Dry Air", *Journal of Physics D: Applied Physics*, Vol.31, pp. 1100-1108, 1998.

[24] N.L. Aleksandrov, E.M. Bazelyan, V.A. Vasil'ev, "The effect of low direct voltage on streamer breakdown in long non-uniform air-gaps", *Journal of Physics D: Applied Physics*, Vol. 36, pp. 2089-2095, 2003.

[25] N.L. Aleksandrov, E.M. Bazelyan, I.V. Kochetov, and N.A. Dyatko, "The Ionisation Kinetics and Electric Field in the Leader Channel in Long Air Gaps", *Journal of Physics D: Applied Physics*, Vol. 30, pp. 1616-1624, 1997.

[26] A. Pigini, L. Thione, and F. Rizk, "Dielectric Strength under AC and DC Voltages", *Cigre Working Group 33.03.07*, Guidelines for the Evaluation of the dielectric strength of external Insulation, Paris, 1993, pp. 47-51.

[27] N. Knudsen, and F. Iliceto, "Flashover Tests on Large Air Gaps with DC Voltage and with Switching Surges superimposed on DC Voltage", *IEEE Transactions on Power Apparatus and Systems*, Vol. 89, No. 5, pp. 781-788, 1970.

[28] H.L. Hill, P.E. Renner, M.G. Poland, and W.E. Scarborough, "BPA's Extra-High-Voltage DC tests, Part 2: Outdoor Flashover", *IEEE Transactions on Power Apparatus and Systems*, Vol. 86, No. 10, pp. 1153-1160, 1967.

[29] Transmission Line Reference Book, HVDC to ± 600 kV, EPRI, Chapter 10: Clearances.

[30] D.V. Razevig, "High Voltage Engineering", Khanna Publishers, 1978, p. 88.

[31] International Electrotechnical Commission, *High Voltage Test Techniques*, Part 1: General Definitions and Test Requirements, IEC 60060-1.

[32] N.L. Allen, J.R. Fonesca, H.J. Geldenhuys and J.C. Zheng, "Influence of Air Humidity on the Dielectric Strength of External Insulation", *Cigre Working Group 33.03.07*, Guidelines for the Evaluation of the dielectric strength of external Insulation, Paris, 1993, pp. 57-64.

[33] Task Force 07.03 of Study Committee 33, Humidity Influence on Non-Uniform Field Breakdown in Air, Cigre Electra No. 134,

[34] HVDC Test Set Instruction Manual, MWB India Limited, 2000.

[35] Personal communication with H.F. Vosloo, November 2006.

[36] Personal communication with A.C. Britten, January 2007.